Accepted Manuscript

On the high temperature mechanical behaviors analysis of heated functionally graded plates using FEM and a new third-order shear deformation plate theory

Tinh Quoc Bui, Thom Van Do, Lan Hoang That Ton, Duc Hong Doan, Satoyuki Tanaka, Dat Tien Pham, Thien-An Nguyen-Van, Tiantang Yu, Sohichi Hirose

PII: S1359-8368(16)00162-1

DOI: 10.1016/j.compositesb.2016.02.048

Reference: JCOMB 4086

To appear in: *Composites Part B*

Received Date: 20 August 2015

Revised Date: 28 December 2015

Accepted Date: 18 February 2016

Please cite this article as: Bui TQ, Do TV, Ton LHT, Doan DH, Tanaka S, Pham DT, Nguyen-Van T-A, Yu T, Hirose S, On the high temperature mechanical behaviors analysis of heated functionally graded plates using FEM and a new third-order shear deformation plate theory, *Composites Part B* (2016), doi: 10.1016/j.compositesb.2016.02.048.

On the high temperature mechanical behaviors analysis of heated functionally graded plates using FEM and a new third-order shear deformation plate theory

Tinh Quoc Bui[a,*,†], Thom Van Do[b], Lan Hoang That Ton[c], Duc Hong Doan[d], Satoyuki Tanaka[e], Dat Tien Pham[b], Thien-An Nguyen-Van[f], Tiantang Yu[g], Sohichi Hirose[a]

[a]*Department of Mechanical and Environmental Informatics, Tokyo Institute of Technology, 2-12-1-W8-22, Ookayama, Meguro-ku, Tokyo 152-8552, Japan.*

[b]*Department of Mechanics, Le Quy Don Technical University, 236 Hoang Quoc Viet, Hanoi, Vietnam.*

[c]*Department of Civil Engineering, Ho Chi Minh City University of Architecture, Vietnam*

[d]*Department of Mechanical and Control Engineering, Tokyo Institute of Technology, Japan*

[e]*Graduate School of Engineering, Hiroshima University, Japan*

[f]*Department of Technical Education, Danang University of Science and Technology, The University of Danang, Vietnam*

[g]*Department of Engineering Mechanics, Hohai University, Nanjing, PR China*

[*] Corresponding authors: T. Q. Bui, Department of Mechanical and Environmental Informatics, Tokyo Institute of Technology, 2-12-1-W8-22, O-okayama, Meguro-ku, Tokyo 152-8552, Japan

Tel: +81 (0)7021506399

[†] E-mail: tinh.buiquoc@gmail.com

Highlight

- New numerical results of mechanical behaviors of FG plates in high temperature are presented.
- A finite element model based on a new third-order shear deformation plate theory is developed.
- Not all FGMs possess similar mechanical behaviors and performance in high temperature.
- Similar behaviors of natural frequencies in high temperature of FGMs are found
- Material combinations of FGMs play a key role and significantly affect the mechanical behaviors of plates.

Abstract

Composite functionally graded materials (FGMs) are fabricated and most commonly used to operate in high temperature environments, where are expected to have significant changes in properties of constituent materials. The FGMs inherently withstand high temperature gradients due to low thermal conductivity, core ductility, low thermal expansion coefficient, and many others. It is essential to thoroughly study mechanical responses of FGMs and to develop new effective approaches for accurate prediction of solutions. We present in this paper new numerical results of high temperature mechanical behaviors of heated functionally graded (FG) plates, emphasizing the high temperature effects on static bending deflections and natural frequencies. A displacement-based finite element formulation associated with a novel third-order shear deformation plate theory (TSDT) without any requirement of shear correction factors is thus developed, taking the desirable properties and advantages of the TSDT theory as its kinematics of displacements are derived from elasticity theory rather than the hypothesis of displacement. The FG plates are assumed to be placed suffering high temperature environment, resulting in a uniform distribution of temperature across the plate thickness. The variation of material compositions across the thickness is described by a power-law distribution. Representative numerical examples of heated FG plates with different shapes are considered and obtained results are then investigated. The work additionally involves parametric studies performed by varying volume fraction, temperature range, material combinations, thickness-to-length ratio, etc., which have significant impacts on mechanical deflections and natural frequencies of heated FG plates. It is found that the ZrO_2/SUS304 plate possesses different static bending behaviors and performance compared to Al_2O_3/SUS304 and Si_3N_4/SUS304 plates due to the differences not only in the nonlinear thermal expansions but also in the material behaviors of constituent materials by which the FGMs are formed, in the contrary similar behaviors of natural frequencies of all FG plates is found.

Keywords: *Functionally graded materials; Finite element analysis (FEA); Vibration; Third-order shear deformation theory; Plates; High temperature properties.*

1. Introduction

Composite materials with graded microstructures or functionally graded materials (FGMs), which are characterized by gradual variation of effective material properties and spatially varied non-uniform microstructures of constituent phases (as schematically illustrated in Fig. 1 [1] for NiCoCrAIY-YSZ), have been successfully manufactured, developed and designed in a wide range of engineering applications that most commonly operate in situations suffering high temperature environments. The FGMs are usually made from a mixture of ceramic (e.g., YSZ) and metal (e.g., NiCoCrAIY), gaining a smooth and continuous variation of material properties from one surface to another throughout specific directions [2]. Due to their outstanding features and excellent characteristics of ceramics in heat and corrosive resistance, and the high toughness of metal in absorb energy and plastically deform, the FGMs particularly are capable of withstanding intense high temperature gradient but maintaining the structural integrity as well as eliminating/reducing interface problems, thermal stress concentration, residual stresses, and so on [3]. The FGMs specially have now gained much more attention in high temperature applications, especially in nuclear plants, fusion reactors and spacecraft [4]. For instance, a useful and technical application of the FGMs is the thermal barrier coatings (TBCs), which are generated for the purpose of increasing the service life and performance of structures. The TBCs can not only provide thermal resistance to metallic substrates, but also reduce the substrate surface temperatures, which can be applied to many power generation systems like gas turbines, diesel engines, aircraft engines, and so on [1].

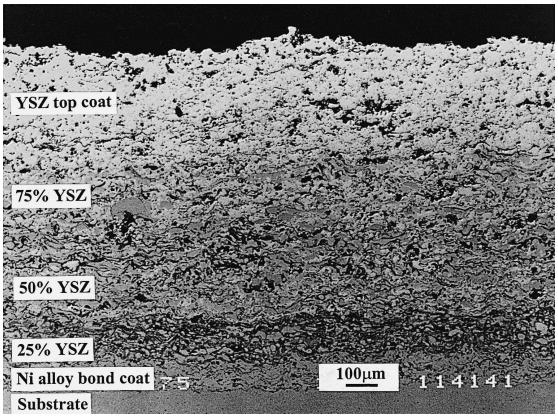

Fig. 1 NiCoCrAIY-YSZ composite five-layered functionally graded material [1], exhibiting graded microstructures and representing a smooth and continuous variation of material properties from one surface to another throughout specific directions.

In line of significantly increasing in use of the FGMs for many engineering applications nowadays, further studies for a better and thorough understanding in material behaviors and mechanical response of structures made of FGMs suffering high temperature environments are important. In many aforementioned engineering applications, valuable knowledge regarding the mechanical behaviors of FGMs plays an important role in the design and development of new products. Keeping track of the preceding studies of FG plates in terms of thermal conditions has shown that there are a great deal of works accounting for the behaviors of FG plates subjected to various mechanical and thermal loadings. Wattanasakulpong et al. [3, 5] formulated analytical solutions for free, forced vibration and thermal buckling analysis of FG beams and plates under high temperature, respectively, using a new simple third-order shear deformation plate theory [4]. Shen and his co-workers [4, 7-9] analytically presented nonlinear solutions of bending, vibration and dynamic responses of FG plates in thermal environments using high-order shear deformation plate theories. Under ambient or room temperature, Talha and Singh reported static response and

free vibration of FG plates with different boundary conditions based on finite element method (FEM) and a high-order theory [10]. Transient thermal stresses in FG plates induced by unsteady heat conduction, temperature-dependent material properties are examined by Tanigawa et al. [11]. Shariat and Eslami [12] proposed closed-form solutions of thermal buckling of imperfect FG plates using the classical plate theory, while a new micromechanical theory for the response of FG metal-matrix composites subjected to thermal gradients is developed by Aboudi et al. [13]. Kim and Noda [14] described a Green's function approach to the deflection of FG plates under transient thermal loading. Recently, Golmakani et al. [15] explored large deformation of circular and annular FGM plates under thermo-mechanical loadings with temperature-dependent properties, using the first-order shear deformation theory and von Karman description.

It is obvious that most preceding efforts are devoted to the solutions that are derived from the analytical or closed-form approaches, whereas solutions based on the numerical methods like FEM for mechanical response of FG plates in high temperature are rather rare. The analytical solutions are useful in some particular cases, but they are very limited in general, especially in practice where complicated geometries and boundary and loading conditions or others like high temperature environments are often encountered. In light of that circumstance, the present work particularly intends to fill that gap by providing an effective numerical model, which is based on a displacement-based finite element formulation integrating with a new improved third-order shear deformation plate theory, for mechanical response of static bending and natural frequencies of heated FG plates under high temperature environment. Compared to analytical approaches, the work being studied is expected to serve a more general purpose of numerical modeling of heated FG plates suffering high temperature environment.

Many different plate theories from the classical to high order ones have developed in the past few decades, curious readers may refer to, e.g., see [16, 17], for more information on recent developments of the plate theories. However, it reveals one important conclusion that the third-order shear deformation plate theories (TSDTs) are one of the effective and accurate methods available in literature due to the fact that the TSDTs account for a quadratic variation of the transverse shear strains and stresses across the thickness, and more importantly the shear correction factors are no long required in most TSDTs as well as high accuracy on the stress distributions can be obtained. The TSDTs may be highly suitable for capturing the inherent nonlinear properties of FGMs as the field variables of displacements are often expressed in terms of cubic functions of the thickness coordinates. Recently, Shi [6] successfully formulated a novel improved yet simple third-order shear deformation plate theory (TSDT) based on rigorous kinematics of displacements, initially applied to static analysis of isotropic and orthotropic beams and plates. The results obtained by the Shi’s TSDT have shown to be more reliable and highly accurate than many other higher-order shear deformation plate theories. The achievement of higher accuracy of the Shi’s TSDT may be due to the fact that the kinematics of displacement is derived from elasticity theory rather the hypothesis of displacement like other existing approaches. Only a few works have developed based on the Shi's TSDT, for instance, Wattanasakupong et al. [3, 5] adopted the Shi’s TSDT to analytically develop exact solutions for thermal buckling and elastic vibration of FG beams and free and forced vibration of FG plates in high temperature. Therefore, the Shi’s TSDT is relatively young, new and its application and extension to other models/problems is potential. The present work is thus the first development of forming the Shi's TSDT into a numerical model in terms of finite element analysis, which is

expected to be an effect numerical tool highly suitable for practical applications.

Formulating a new and effective displacement-based finite element model, taking the outstanding features of the Shi's TSDT into account, for extracting mechanical response of static bending and natural frequencies of FG plates in high temperature environments with different configurations is one of the main objectives of the present study. We emphasize our attention on the accuracy of the proposed TSDT-based FE approach, and addressing new numerical results of mechanical response of heated FG plates in high temperature in which the effect of high temperature conditions on the static deflections and natural frequencies is explored. We highlight the parametric studies performed by varying volume fraction, material combinations, plate thickness-to-length ratio, boundary conditions, etc., which have great impacts on mechanical response of heated FG plates. In this study, the FG plates are assumed to be placed in a high temperature environment for a long period and the temperature hence distributes uniformly across the plate thickness. The gradual variation of effective material compositions throughout the thickness is represented by a power law distribution. Representative numerical examples of heated FG plates with different configurations involving a square, a circle and an L-shape are considered and obtained results are then verified and investigated in detail.

Additionally, the FG plates are one of the major research interests of the authors and hence several works have been recently studied, for instance, buckling failure analysis of cracked FGM plates using a discrete shear gap 3-node extended finite element [2]; geometrically linear and nonlinear of FGM plates using the first order shear deformation theory and isogeometric analysis [18-21]; mechanical response of cracked FG plates under different loads and boundary conditions derived from an XIGA [22]; a quasi-3D hypothesis shear deformation theory for FG

plates; dynamic transient analysis of sandwich beams with FG core using a novel truly meshfree method [23], and so on. As a consequence, conditions under making use of our previous knowledge, computer resources and experience are great advantages to make this work to appear.

The rest of the manuscript is structured as follows. We briefly present in Section 2 the fundamental of functionally graded material plates, highlighting the effective material properties under thermal conditions. Finite element formulation for mechanical responses of static bending and free vibration problems of heated FG plates is developed and presented in Section 3. Section 4 shows the numerical results of static bending deflections and natural frequencies for three heated FG plates with different configurations, and a discussion on the static bending deflections and natural frequencies under high temperature is given. Some conclusions drawn from the study are presented in the last section.

2. Functionally graded plates

Material properties of FG plates are usually assumed to be varied in the volume fractions in the plate thickness. Let us consider a ceramic-metal FG plate with thickness *h* as depicted in Fig. 2, assuming that its bottom and top faces are to be fully metallic and ceramic, respectively. The *xy*-plane is the mid-plane of the plate, while the positive *z*-axis is upward from the mid-plane. There are some descriptions to the variation of the volume fractions available in the literature, and in this particular work we adopt the common simple power-law assumption for describing the volume fraction of the ceramic (V_c) and the metal (V_m) [2, 24]:

$$V_c = \left(\frac{z}{h} + \frac{1}{2}\right)^n ; \quad V_m = 1 - V_c \quad \text{with} \quad n \geq 0 \tag{1}$$

where z is the thickness coordinate variable with $-h/2 \leq z \leq h/2$, and subscripts c and m

represent the ceramic and metal constituents, respectively. In this paper, we denote *n* being the non-negative volume fraction gradient index and its variation can greatly alter the material properties as schematically sketched in Fig. 3. Particularly, it is easy to obtain a pure ceramic material by setting $n=0$, whereas a pure metal by assigning $n=\infty$.

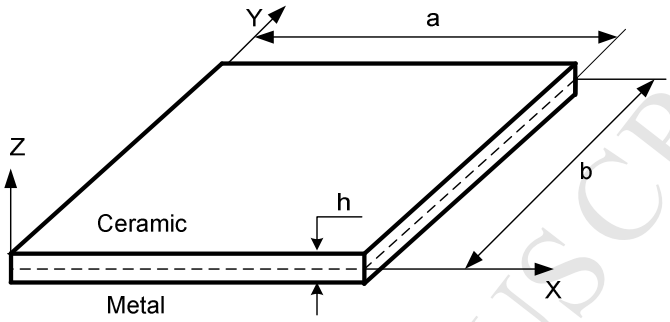

Fig. 2 Geometrical notation of a rectangular FG plate.

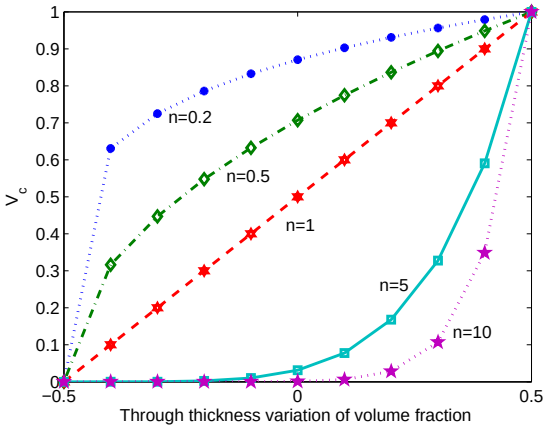

Fig. 3 Variation of volume fraction with respect to the non-dimensional thickness for various non-negative volume fraction coefficients of an FG plate using the power-law distribution.

The Young's modulus *E*, the density ρ, the Poisson's ratio ν, and the coefficient of thermal expansion α vary through the thickness with a power-law distribution [3, 4, 7-9]:

$$E(z)=E_m+(E_c-E_m)\left(\frac{1}{2}+\frac{z}{h}\right)^n$$
$$\rho(z)=\rho_m+(\rho_c-\rho_m)\left(\frac{1}{2}+\frac{z}{h}\right)^n \tag{2}$$

$$\nu(z) = \nu_m + (\nu_c - \nu_m)\left(\frac{1}{2} + \frac{z}{h}\right)^n$$

$$\alpha(z) = \alpha_m + (\alpha_c - \alpha_m)\left(\frac{1}{2} + \frac{z}{h}\right)^n$$

Environments under study where the common use of FG plates suffers high temperature often induce considerable changes in material properties. The effect of temperature on material properties must hence be taken into account, as a result of the nonlinear equation of themoelastic material properties, which is as a function of temperature *T(K)*, and can be expressed as [3, 4, 7-9, 25, 26]

$$P = P_0\left(P_{-1}T^{-1} + 1 + P_1T + P_2T^2 + P_3T^3\right) \tag{3}$$

where $T = T_0 + \Delta T$ and $T_0 = 300K$ (ambient or free stress temperature), ΔT is the temperature change, and P_0, P_{-1}, P_1, P_2, P_3 are the coefficients of temperature $T(K)$, and are unique to each constituent.

3. Finite element formulation for bending and vibration analysis of FG plates

The goal of this section is to derive a finite element formulation for heated FG plate taking the advantages of a new simple third-order shear deformation plate theory, which is originally proposed by Shi [6] based on rigorous kinematic of displacements. Previous effort presented in [6] has made to reveal the advantages of this new theory as it substantially provides more accuracy than other higher-order shear deformation plate theories. It may be due to the fact that the kinematic of displacements is derived from an elasticity formulation rather than the hypothesis of displacements.

According to the new theory [6], the three-dimensional displacement field (u, v, w) can be expressed in terms of five unknown variables as follows:

$$u(x,y,z)=u_0(x,y)+\frac{5}{4}\left(z-\frac{4}{3h^2}z^3\right)\phi_x(x,y)+\left(\frac{1}{4}z-\frac{5}{3h^2}z^3\right)w_{0,x}$$

$$v(x,y,z)=v_0(x,y)+\frac{5}{4}\left(z-\frac{4}{3h^2}z^3\right)\phi_y(x,y)+\left(\frac{1}{4}z-\frac{5}{3h^2}z^3\right)w_{0,y} \tag{4}$$

$$w(x,y,z)=w_0(x,y)$$

where u_0, v_0, and w_0 define the displacements at the mid-plane of a plate in the *x*, *y*, and *z* directions respectively, while ϕ_x and ϕ_y denote the transverse normal rotations of the *y* and *x* axes. In Eq. (4), the comma represents the differentiation against *x* and *y* coordinates.

Under small strain assumptions, the strain–displacement relations can be expressed as follows:

$$\begin{Bmatrix}\varepsilon_x\\ \varepsilon_y\\ \varepsilon_{xy}\\ \gamma_{yz}\\ \gamma_{xz}\end{Bmatrix}=\begin{Bmatrix} u_{0,x}+z\frac{1}{4}\left(5\phi_{x,x}+w_{,xx}\right)+z^3\left(\frac{-5}{3h^2}\right)\left(\phi_{x,x}+w_{,xx}\right)\\ v_{0,y}+z\frac{1}{4}\left(5\phi_{y,y}+w_{,yy}\right)+z^3\left(\frac{-5}{3h^2}\right)\left(\phi_{y,y}+w_{,yy}\right)\\ u_{0,y}+v_{0,x}+z\frac{1}{4}\left(5\phi_{x,y}+2w_{,xy}+5\phi_{y,x}\right)+z^3\left(\frac{-5}{3h^2}\right)\left(\phi_{x,y}+2w_{,xy}+\phi_{y,x}\right)\\ \frac{5}{4}\left(\phi_y+w_{,y}\right)+z^2\left(\frac{-5}{h^2}\right)\left(\phi_y+w_{,y}\right)\\ \frac{5}{4}\left(\phi_x+w_{,x}\right)+z^2\left(\frac{-5}{h^2}\right)\left(\phi_x+w_{,x}\right)\end{Bmatrix} \tag{5}$$

or in matrix form

$$\begin{Bmatrix}\boldsymbol{\varepsilon}\\ \boldsymbol{\gamma}\end{Bmatrix}=\begin{Bmatrix}\boldsymbol{\varepsilon}^{(0)}\\ \boldsymbol{\gamma}^{(0)}\end{Bmatrix}+\mathbf{z}\begin{Bmatrix}\boldsymbol{\varepsilon}^{(1)}\\ 0\end{Bmatrix}+\mathbf{z}^2\begin{Bmatrix}0\\ \boldsymbol{\gamma}^{(2)}\end{Bmatrix}+\mathbf{z}^3\begin{Bmatrix}\boldsymbol{\varepsilon}^{(3)}\\ 0\end{Bmatrix} \tag{6}$$

in which

$$\boldsymbol{\varepsilon}^{(0)}=\begin{Bmatrix}u_{0,x}\\ v_{0,y}\\ u_{0,y}+v_{0,x}\end{Bmatrix};\quad \boldsymbol{\varepsilon}^{(1)}=\frac{1}{4}\begin{Bmatrix}\left(5\phi_{x,x}+w_{,xx}\right)\\ \left(5\phi_{y,y}+w_{,yy}\right)\\ \left(5\phi_{x,y}+2w_{,xy}+5\phi_{y,x}\right)\end{Bmatrix};\quad \boldsymbol{\varepsilon}^{(3)}=\frac{-5}{3h^2}\begin{Bmatrix}\phi_{x,x}+w_{,xx}\\ \phi_{y,y}+w_{,yy}\\ \phi_{x,y}+2w_{,xy}+\phi_{y,x}\end{Bmatrix} \tag{7}$$

$$\boldsymbol{\gamma}^{(0)}=\frac{5}{4}.\begin{Bmatrix}\phi_y+w_{,y}\\ \phi_x+w_{,x}\end{Bmatrix};\quad \boldsymbol{\gamma}^{(2)}=\frac{-5}{h^2}\begin{Bmatrix}\phi_y+w_{,y}\\ \phi_x+w_{,x}\end{Bmatrix} \tag{8}$$

The constitutive relations are derived from Hooke's law by the following equation:

$$\boldsymbol{\sigma}=\mathbf{D}_m(\mathbf{z})(\boldsymbol{\varepsilon}^{(0)}+\mathbf{z}\boldsymbol{\varepsilon}^{(1)}+\mathbf{z}^3\boldsymbol{\varepsilon}^{(3)}-\boldsymbol{\varepsilon}^{(T)}) \tag{9}$$

$$\boldsymbol{\tau} = \mathbf{D}_s(z)\left(\boldsymbol{\gamma}^{(0)} + \mathbf{z}^2\boldsymbol{\gamma}^{(2)}\right)$$

with

$$\boldsymbol{\sigma} = \begin{bmatrix} \sigma_x & \sigma_y & \sigma_{xy} \end{bmatrix}^{\mathrm{T}};\ \boldsymbol{\tau} = \begin{bmatrix} \tau_{yz} & \tau_{xz} \end{bmatrix}^{\mathrm{T}} \tag{10a}$$

$$\mathbf{D}_m(z) = \frac{E(z)}{1-\nu^2}\begin{bmatrix} 1 & \nu & 0 \\ \nu & 1 & 0 \\ 0 & 0 & (1-\nu)/2 \end{bmatrix} \tag{10b}$$

$$\mathbf{D}_s(z) = \frac{E(z)}{2(1+\nu)}\begin{bmatrix} 1 & 0 \\ 0 & 1 \end{bmatrix} \tag{10c}$$

$$\boldsymbol{\varepsilon}^{(T)} = \begin{bmatrix} \boldsymbol{\varepsilon}_x^{(T)} & \boldsymbol{\varepsilon}_y^{(T)} & \mathbf{0} \end{bmatrix}^{\mathrm{T}} = \alpha(z)\Delta T\begin{bmatrix} 1 & 1 & 0 \end{bmatrix}^{\mathrm{T}} \tag{10d}$$

It must be noted in all above equations that we have denoted $\boldsymbol{\varepsilon}^{(T)}$ to indicate the strain induced by temperature, which is different from the term of transpose, i.e., $(\cdot)^{\mathrm{T}}$.

In this study, we adopt a quadrilateral 4-node plate element in which each node contains five degrees of freedom, i.e., $q_{ie} = \{u_{0i} \quad v_{0i} \quad w_i \quad \phi_{xi} \quad \phi_{yi}\}^{\mathrm{T}}$, $i = 1-4$. The generalized displacements in the middle plane can hence be approximated as

$$\mathbf{u}_0 = \mathbf{N}\mathbf{q}_e \tag{11}$$

with

$$\mathbf{u}_0 = \begin{bmatrix} u_0 & v_0 & w & \phi_x & \phi_y \end{bmatrix}^{\mathrm{T}} \tag{12a}$$

$$\mathbf{N} = \begin{bmatrix} N_1 & N_2 & N_3 & N_4 \end{bmatrix} \tag{12b}$$

$$\mathbf{q}_e = \begin{bmatrix} \mathbf{q}_{1e} & \mathbf{q}_{2e} & \mathbf{q}_{3e} & \mathbf{q}_{4e} \end{bmatrix}^{\mathrm{T}} \tag{12c}$$

where $\mathbf{N}$ and $\mathbf{q}_e$ denote the shape function and the unknown displacement vector at element, respectively.

By substituting Eq. (11) into Eqs. (7) and (8), the strain can be obtained as follows:

$$\begin{aligned} \boldsymbol{\varepsilon} &= \left(\mathbf{B}_1 + \mathbf{B}_2 + \mathbf{B}_3\right)\mathbf{q}_e; \\ \boldsymbol{\gamma} &= \left(\mathbf{B}_4 + \mathbf{B}_5\right)\mathbf{q}_e \end{aligned} \tag{13}$$

with

$$\mathbf{B}_1=\sum_{i=1}^{4}\begin{bmatrix}\mathbf{N}_{i,x} & \mathbf{0} & \mathbf{0} & \mathbf{0} & \mathbf{0}\\ \mathbf{0} & \mathbf{N}_{i,y} & \mathbf{0} & \mathbf{0} & \mathbf{0}\\ \mathbf{N}_{i,y} & \mathbf{N}_{i,x} & \mathbf{0} & \mathbf{0} & \mathbf{0}\end{bmatrix};\ \mathbf{B}_2=\frac{1}{4}\sum_{i=1}^{4}\begin{bmatrix}\mathbf{0} & \mathbf{0} & \mathbf{N}_{i,xx} & 5\mathbf{N}_{i,x} & \mathbf{0}\\ \mathbf{0} & \mathbf{0} & \mathbf{N}_{i,yy} & \mathbf{0} & 5\mathbf{N}_{i,y}\\ \mathbf{0} & \mathbf{0} & 2\mathbf{N}_{i,xy} & 5\mathbf{N}_{i,y} & 5\mathbf{N}_{i,x}\end{bmatrix};$$
$$\mathbf{B}_3=\frac{5}{3h^2}\sum_{i=1}^{4}\begin{bmatrix}\mathbf{0} & \mathbf{0} & \mathbf{N}_{i,xx} & \mathbf{N}_{i,x} & \mathbf{0}\\ \mathbf{0} & \mathbf{0} & \mathbf{N}_{i,yy} & \mathbf{0} & \mathbf{N}_{i,y}\\ \mathbf{0} & \mathbf{0} & 2\mathbf{N}_{i,xy} & \mathbf{N}_{i,y} & \mathbf{N}_{i,x}\end{bmatrix} \tag{14a}$$

and

$$\mathbf{B}_4=\frac{5}{4}\sum_{i=1}^{4}\begin{bmatrix}\mathbf{0} & \mathbf{0} & \mathbf{N}_{i,y} & \mathbf{0} & \mathbf{1}\\ \mathbf{0} & \mathbf{0} & \mathbf{N}_{i,x} & \mathbf{1} & \mathbf{0}\end{bmatrix};\mathbf{B}_5=\frac{5}{h^2}\sum_{i=1}^{4}\begin{bmatrix}\mathbf{0} & \mathbf{0} & \mathbf{N}_{i,y} & \mathbf{0} & \mathbf{1}\\ \mathbf{0} & \mathbf{0} & \mathbf{N}_{i,x} & \mathbf{1} & \mathbf{0}\end{bmatrix} \tag{14b}$$

The normal forces, bending moments, higher-order moments and shear force can then be computed through the following relations

$$\tilde{\mathbf{N}}=\left\{\tilde{N}_x\ \ \tilde{N}_y\ \ \tilde{N}_{xy}\right\}^{\mathrm{T}}=\int_{-h/2}^{h/2}\left\{\sigma_x\ \ \sigma_y\ \ \sigma_{xy}\right\}^{\mathrm{T}}dz=$$
$$=\int_{-h/2}^{h/2}\mathbf{D}_m(z)\left(\boldsymbol{\varepsilon}^{(0)}+z\boldsymbol{\varepsilon}^{(1)}+z^3\boldsymbol{\varepsilon}^{(3)}-\boldsymbol{\varepsilon}^{(T)}\right)dz \tag{15a}$$

$$\tilde{\mathbf{M}}=\left\{\tilde{M}_x\ \ \tilde{M}_y\ \ \tilde{M}_{xy}\right\}^{\mathrm{T}}=\int_{-h/2}^{h/2}\left\{\sigma_x\ \ \sigma_y\ \ \sigma_{xy}\right\}^{\mathrm{T}}zdz=$$
$$=\int_{-h/2}^{h/2}\mathbf{D}_m(z)\left(\boldsymbol{\varepsilon}^{(0)}+z\boldsymbol{\varepsilon}^{(1)}+z^3\boldsymbol{\varepsilon}^{(3)}-\boldsymbol{\varepsilon}^{(T)}\right)zdz \tag{15b}$$

$$\tilde{\mathbf{P}}=\left\{\tilde{P}_x\ \ \tilde{P}_y\ \ \tilde{P}_{xy}\right\}^{\mathrm{T}}=\int_{-h/2}^{h/2}\left\{\sigma_x\ \ \sigma_y\ \ \sigma_{xy}\right\}^{\mathrm{T}}z^3dz\ =$$
$$=\int_{-h/2}^{h/2}\mathbf{D}_m(z)\left(\boldsymbol{\varepsilon}^{(0)}+z\boldsymbol{\varepsilon}^{(1)}+z^3\boldsymbol{\varepsilon}^{(3)}-\boldsymbol{\varepsilon}^{(T)}\right)z^3dz \tag{15c}$$

$$\tilde{\mathbf{Q}}=\left\{\tilde{Q}_y\ \ \tilde{Q}_x\right\}^{\mathrm{T}}=\int_{-h/2}^{h/2}\left\{\tau_{yz}\ \ \tau_{xz}\right\}^{\mathrm{T}}dz=\int_{-h/2}^{h/2}\mathbf{D}_s(z)\left(\boldsymbol{\gamma}^{(0)}+z^2\boldsymbol{\gamma}^{(2)}\right)dz \tag{15d}$$

$$\tilde{\mathbf{R}}=\left\{\tilde{R}_y\ \ \tilde{R}_x\right\}^{\mathrm{T}}=\int_{-h/2}^{h/2}\left\{\tau_{yz}\ \ \tau_{xz}\right\}^{\mathrm{T}}z^2dz\ =\int_{-h/2}^{h/2}\mathbf{D}_s(z)\left(\boldsymbol{\gamma}^{(0)}+z^2\boldsymbol{\gamma}^{(2)}\right)z^2dz \tag{15e}$$

Eq. (15) can be rewritten in matrix form

$$\begin{Bmatrix} \tilde{\mathbf{N}} \\ \tilde{\mathbf{M}} \\ \tilde{\mathbf{P}} \\ \tilde{\mathbf{Q}} \\ \tilde{\mathbf{R}} \end{Bmatrix} = \begin{bmatrix} \mathbf{A} & \mathbf{B} & \mathbf{E} & \mathbf{0} & \mathbf{0} \\ \mathbf{B} & \mathbf{D} & \mathbf{F} & \mathbf{0} & \mathbf{0} \\ \mathbf{E} & \mathbf{F} & \mathbf{H} & \mathbf{0} & \mathbf{0} \\ \mathbf{0} & \mathbf{0} & \mathbf{0} & \hat{\mathbf{A}} & \hat{\mathbf{B}} \\ \mathbf{0} & \mathbf{0} & \mathbf{0} & \hat{\mathbf{B}} & \hat{\mathbf{D}} \end{bmatrix} \begin{Bmatrix} \boldsymbol{\varepsilon}^{(0)} \\ \boldsymbol{\varepsilon}^{(1)} \\ \boldsymbol{\varepsilon}^{(3)} \\ \boldsymbol{\gamma}^{(0)} \\ \boldsymbol{\gamma}^{(2)} \end{Bmatrix} - \begin{Bmatrix} \tilde{\mathbf{N}}^{(T)} \\ \tilde{\mathbf{M}}^{(T)} \\ \tilde{\mathbf{P}}^{(T)} \\ \mathbf{0} \\ \mathbf{0} \end{Bmatrix} \tag{16}$$

with

$$\left(\mathbf{A},\ \mathbf{B},\ \mathbf{D},\ \mathbf{E},\ \mathbf{F},\ \mathbf{H}\right) = \int_{-h/2}^{h/2} \left(1,\ z,\ z^2,\ z^3,\ z^4,\ z^6\right) \mathbf{D}_m(z)\, dz \tag{17a}$$

$$\left(\hat{\mathbf{A}},\ \hat{\mathbf{B}},\ \hat{\mathbf{D}}\right) = \int_{-h/2}^{h/2} \left(1,\ z^2,\ z^4\right) \mathbf{D}_s(z)\, dz \tag{17b}$$

$$\left(\tilde{\mathbf{N}}^{(T)},\ \tilde{\mathbf{M}}^{(T)}, \tilde{\mathbf{P}}^{(T)}\right) = \int_{-h/2}^{h/2} \mathbf{D}_m(z) \left(1,\ z,\ z^3\right) \{1\ \ 1\ \ 0\}^{\mathrm{T}}\, \alpha(z) \Delta T\, dz \tag{17c}$$

It is interesting to see that Eqs. (16) and (17) reveal the thermal stresses that take place in the behaviors of the heated FG plates.

As we have already stated in the previous section that the FG plates under consideration are assumed to be placed in high temperature environment for a long period. The temperature is hence assumed to be uniformly distributed across the plate thickness. The variation of the temperature within the FG plates is controlled by the temperature change ΔT.

The total strain energy of a plate due to the normal forces, shear force, bending moments and higher-order moments can be given by

$$\begin{aligned} U = \frac{1}{2}\int_{V_e} \boldsymbol{\varepsilon}^{\mathrm{T}} \boldsymbol{\sigma}\, dV - \int_{S_e} \mathbf{u}^{\mathrm{T}} \mathbf{f}\, dS = \frac{1}{2}\mathbf{q}_e^{\mathrm{T}} \int_{S_e} \begin{pmatrix} \mathbf{B}_1^{\mathrm{T}}\mathbf{A}\mathbf{B}_1 + \mathbf{B}_1^{\mathrm{T}}\mathbf{B}\mathbf{B}_2 + \mathbf{B}_1^{\mathrm{T}}\mathbf{E}\mathbf{B}_3 + \\ + \mathbf{B}_2^{\mathrm{T}}\mathbf{B}\mathbf{B}_1 + \mathbf{B}_2^{\mathrm{T}}\mathbf{D}\mathbf{B}_2 + \mathbf{B}_2^{\mathrm{T}}\mathbf{F}\mathbf{B}_3 + \\ + \mathbf{B}_3^{\mathrm{T}}\mathbf{E}\mathbf{B}_1 + \mathbf{B}_3^{\mathrm{T}}\mathbf{F}\mathbf{B}_2 + \mathbf{B}_3^{\mathrm{T}}\mathbf{H}\mathbf{B}_3 + \\ + \mathbf{B}_4^{\mathrm{T}}\hat{\mathbf{A}}\mathbf{B}_4 + \mathbf{B}_4^{\mathrm{T}}\hat{\mathbf{B}}\mathbf{B}_5 + \mathbf{B}_5^{\mathrm{T}}\hat{\mathbf{B}}\mathbf{B}_4 + \\ + \mathbf{B}_5^{\mathrm{T}}\hat{\mathbf{D}}\mathbf{B}_5 \end{pmatrix} dS\mathbf{q}_e - \\ - \mathbf{q}_e^{\mathrm{T}} \int_{S_e} \left(\mathbf{B}_1^{\mathrm{T}}\tilde{\mathbf{N}}^{(T)} + \mathbf{B}_2^{\mathrm{T}}\tilde{\mathbf{M}}^{(T)} + \mathbf{B}_3^{\mathrm{T}}\tilde{\mathbf{P}}^{(T)}\right) dS - \mathbf{q}_e^{\mathrm{T}} \int_{S_e} \tilde{\mathbf{N}}^{\mathrm{T}} \mathbf{f}\, dS + \frac{1}{2}\int_{S_e} \left(\boldsymbol{\varepsilon}^{(T)}\right)^{\mathrm{T}} \mathbf{A}\boldsymbol{\varepsilon}^{(T)} dS \end{aligned} \tag{18}$$

where $\mathbf{f}$ is the transverse loading per unit area and Eq. (18) can be rewritten in matrix form as

$$U = \frac{1}{2}\mathbf{q}_e^{\mathrm{T}}\mathbf{K}_e\mathbf{q}_e \; - \; \mathbf{q}_e^{\mathrm{T}}\mathbf{F}_e^{(T)} - \mathbf{q}_e^{\mathrm{T}}\mathbf{F}_e + \mathbf{C}^{(T)} \tag{19a}$$

$$U = \mathbf{q}_e^{\mathrm{T}}\left(\frac{1}{2}\mathbf{K}_e\mathbf{q}_e \; - \; \mathbf{F}_e^{(T)} - \mathbf{F}_e\right) + \mathbf{C}^{(T)} \tag{19b}$$

with $\mathbf{K}_e$ and $\mathbf{F}_e^{(T)}$ defined in Eq. (19) being the element stiffness matrix and the coefficient matrix of temperature change, respectively, whilst $\mathbf{F}_e$ representing the element force vector. In addition, $\mathbf{C}^{(T)} = \frac{1}{2}\int_{S_e}\left(\boldsymbol{\varepsilon}^{(T)}\right)^{\mathrm{T}}\mathbf{A}\boldsymbol{\varepsilon}^{(T)}dS$ is a constant matrix dependent on the temperature but not on the nodal displacement. It must be noticed that the appearance of the temperature-dependent constant matrix $\mathbf{C}^{(T)}$ in the system comes up naturally, as a result of the mathematical manipulation between the stress and strain components at the state of establishing the discrete equations. However, this term disappears and eventually does not present in the final system of discrete equations.

For free vibration analysis of plates, the kinetic energy is expressed as

$$T = \frac{1}{2}\int_{V_e}\dot{\mathbf{u}}^{\mathrm{T}}\boldsymbol{\rho}(z)\dot{\mathbf{u}}dV = \frac{1}{2}\dot{\mathbf{q}}_e^{\mathrm{T}}\left\{\int_{V_e}\tilde{\mathbf{N}}^{\mathrm{T}}\mathbf{L}^{\mathrm{T}}\boldsymbol{\rho}(z)\mathbf{L}\tilde{\mathbf{N}}dV\right\}\dot{\mathbf{q}}_e = \frac{1}{2}\dot{\mathbf{q}}_e^{\mathrm{T}}\mathbf{M}_e\dot{\mathbf{q}}_e \tag{20}$$

In Eq. (20), the dot represents as the differentiation with respect to time. The term $\mathbf{L}$ is explicitly detailed as

$$\mathbf{L} = \begin{bmatrix} 1 & 0 & \left(\frac{1}{4}z - \frac{5}{3h^2}z^3\right)\frac{\partial}{\partial x} & \frac{5}{4}\left(z - \frac{4}{3h^2}z^3\right) & 0 \\ 0 & 1 & \left(\frac{1}{4}z - \frac{5}{3h^2}z^3\right)\frac{\partial}{\partial y} & 0 & \frac{5}{4}\left(z - \frac{4}{3h^2}z^3\right) \\ 0 & 0 & 1 & 0 & 0 \end{bmatrix} \tag{21}$$

and the element mass matrix is hence given by

$$\mathbf{M}_e = \int_{V_e}\tilde{\mathbf{N}}^{\mathrm{T}}\mathbf{L}^{\mathrm{T}}\boldsymbol{\rho}(z)\mathbf{L}\tilde{\mathbf{N}}dV = \int_{S_e}\tilde{\mathbf{N}}^{\mathrm{T}}\left(\int_{-h/2}^{h/2}\boldsymbol{\rho}(z)\mathbf{L}^{\mathrm{T}}\mathbf{L}dz\right)\tilde{\mathbf{N}}dS \tag{22}$$

For bending analysis, the bending solutions can be obtained by solving the following equation:

$$\mathbf{K}\mathbf{d} = \mathbf{F} + \mathbf{F}^{(T)} \tag{23}$$

where $\mathbf{K}$ and $\mathbf{K}^{(T)}$ are the global stiffness matrix and global coefficient matrix of

temperature change, respectively. $\mathbf{F}$ is the global force vector while $\mathbf{d}$ stands for the vector of unknowns.

To obtain the natural frequency, the dynamic equations can be expressed as one must solve the following eigenvalue equation:

$$\left(\mathbf{K}-\omega^2\mathbf{M}\right)\mathbf{d}=0 \tag{24}$$

with ω denoting the natural frequency, and $\mathbf{M}$ representing the global mass matrix.

It should be noted that all the integrations described above are numerically evaluated by using the common Gauss quadrature integration rule.

4. Numerical results and discussion

In this section, we focus our attention on numerical investigations of FEM solutions for static bending deflection and natural frequency of heated FG plates in high temperature environment, exploring the effects of thickness-to-length ratio, different materials, boundary conditions, volume fraction exponent, material combinations, etc. on the mechanical responses. Three representative numerical examples of heated FG plates having different configurations including a rectangular, a circle and an L-shape are considered and analyzed. Both the simply supported and fully clamped boundary conditions are investigated. For the simply supported boundary conditions:

$$v_0 = w = \phi_y = 0 \text{, at } \; x = 0, a \tag{25a}$$

$$u_0 = w = \phi_x = 0 \text{, at } \; y = 0, b \tag{25b}$$

and the fully clamped edges:

$$u_0 = v_0 = w = \phi_x = \phi_y = \partial w/\partial x = \partial w/\partial y = 0 \text{, at } \; x = 0, a \;\text{ and }\; y = 0, b \tag{26}$$

Different material combinations of FG plates made of the ceramics Al_2O_3, Si_3N_4, ZrO_2, and the metal SUS304 with their parameters detailed in Table 1 are studied [3, 4]. In all the

investigations, the numerical results are computed using the proposed finite element model with a regular fine mesh to ensure the accuracy of the final solutions.

Table 1

Temperature dependent coefficient of Young's modulus E (Pa), thermal expansion coefficient α (1/K), Poisson's ratio ν, mass density ρ (kg/m^3) for various materials [3, 4].

Materials	P_0	P_{-1}	P_1	P_2	P_3	P (300K)
Ceramic Aluminum oxide (Al_2O_3)						
E (Pa)	349.55e9	0	-3.853e-4	4.027e-7	-1.673e-10	320.24e9
α (1/K)	6.8269e-6	0	1.838e-4	0	0	7.203e-6
ν	0.26	0	0	0	0	0.260
ρ (kg/m^3)	3800	0	0	0	0	3800
Ceramic silicon nitride (Si_3N_4)						
E (Pa)	348.43e9	0	-3.070e-4	2.160e-7	-8.946e-11	322.27e9
α (1/K)	5.8723e-6	0	9.095e-4	0	0	7.475e-6
ν	0.24	0	0	0	0	0.240
ρ (kg/m^3)	2370	0	0	0	0	2370
Ceramic zironium oxide (ZrO_2)						
E (Pa)	244.27e9	0	-1.371e-3	1.214e-6	-3.681e-10	168.06e9
α (1/K)	12.766e-6	0	-1.491e-3	1.006e-5	-6.778e-11	18.591e-6
ν	0.288	0	1.133e-4		0	0.298
ρ (kg/m^3)	3657	0	0		0	3657
Metal stainless steel SUS304						
E (Pa)	201.04e9	0	3.079e-4	-6.534e-7	0	207.79e9
α (1/K)	12.330e-6	0	8.086e-4	0	0	15.321e-6
ν	0.326	0	-2.002e-4	3.797e-7	0	0.318
ρ (kg/m^3)	8166	0	0	0	0	8166

4.1 Numerical results for static bending analysis

4.1.1 A rectangular FG plate

We start examining the accuracy of the proposed finite element formulation by comparing the obtained numerical results with reference solutions derived from other approaches available in literature. A fully simply supported FG plate (a/b = 1) made of Al/Al_2O_3 with a thickness-to-length aspect ratio of a/h = 10 subjected to a uniform load P is thus considered. The material properties of Al and Al_2O_3, v_m=0.3, E_m=70GPa, and are v_c=0.3, E_c=380GPa, respectively, are employed for the analysis. Fortunately, this particular example has previously studied by other scientists and their results are hence used for the comparison purpose.

For convenience in representation of the numerical results, the maximum central deflection and tensile stress are respectively normalized by

$$\bar{w} = \frac{10h^3 E_c}{Pa^4} w(\frac{a}{2}, \frac{b}{2})$$
$$\bar{\sigma}_{xx} = \frac{h}{Pa} \sigma_{xx}(\frac{a}{2}, \frac{b}{2}, \frac{h}{2}) \quad (27)$$

It must be mentioned here that the Al/Al_2O_3 material used for the analysis of accuracy of the developed FE model is independent of temperature. Table 2 presents a comparison of the normalized deflections and tensile stress of a simply supported FG square plate gained by the developed method and other approaches using different theories such as the Reddy's theory [27], the sinusoidal shear deformation plate theory (SSDPT) [28], and the hyperbolic shear deformation theory (HPSDT) [29]. The results reported in the table are accounted for different values of the volume fraction coefficient, taken from a pure ceramic (n = 0) to a pure metal (n = ∞) as well as others n = 2, 3, 5, and 10. As expected, the present numerical results show a good agreement with other reference solutions for each value of the volume fraction exponent. In

Table 2, the present numerical results clearly reveal a significant effect of the gradient index on both the dimensionless deflections and normal stress of an FG Al/Al_2O_3 plate. As the plate becomes more and more metallic (i.e., the volume fraction index increases), the normalized deflection $\bar{w}$ and the in-plane longitudinal stress $\bar{\sigma}_{xx}$ gradually increase. The same conclusion can interestingly be observed as raised by Daouadji et al. [29] in a way is that the stress $\bar{\sigma}_{xx}$ yields the same values for both the pure ceramic and the pure metal plates. The phenomenon of giving the same values of the stress component for both pure ceramic and metal plates is clear to the authors. It is due to the fact that the material properties of both pure plates are fully homogeneous, in which the modulus of elasticity does not alter the stress distribution. In other words, the stress does not depend on the modulus of elasticity of the homogeneous plates.

Table 2

Comparison of the normalized deflections and tensile stress of a square FG Al/Al_2O_3 plate (a/b = 1, a/h = 10) for different values of the volume fraction exponent n obtained by the present formulation and other approaches: the Reddy's theory [27], the SSDPT [28], and the HPSDT [29].

n	$\bar{w}$				$\bar{\sigma}_{xx}$			
	Reddy [27]	SSDPT [28]	HPSDT [29]	This work	Reddy [27]	SSDPT [28]	HPSDT [29]	This work
Ceramic	0.4665	0.4665	0.4665	0.4630	2.8920	2.8932	2.8928	2.8930
1	0.9421	0.9287	0.9421	0.9130	4.2589	4.4745	4.2607	4.3560
2	1.2227	1.1940	1.2228	1.2069	4.8889	5.2229	4.8890	5.0449
3	1.3530	1.3200	1.3533	1.3596	5.2055	5.6108	5.2064	5.2026
5	1.4646	1.4356	1.4653	1.4874	5.7066	6.1504	5.7074	5.8751
10	1.6054	1.5876	1.6057	1.6308	6.9540	7.3689	6.9547	7.1148
Metal	2.5328	2.5327	2.5327	2.5120	2.8920	2.8932	2.8928	2.8930

We further verify the accuracy of the proposed formulation to the FG plates affected by temperature environment, and thus the temperature under consideration is set to be $T = 300K$ $(\Delta T = 0)$. We employ the same previous simply supported square plate but it is now made of Si_3N_4/SUS304 instead. The material parameters of Si_3N_4/SUS304 for the particular case of $T = 300K$ can be found in Table 1. The maximum central deflections obtained by the present finite element method are normalized by

$$\overline{w} = \frac{100 w_c E_m h^3}{12\left(1-\nu_m^2\right) P a^4} \tag{28}$$

and are then compared with the analytical solutions given by Wattanasakulpong et al. [3], as reported in Table 3. In Eq. (28), E_m and ν_m are the reference values of the Young's modulus and Poisson's ratio of metal at $T = 300K$ detailed in Table 1. A very good agreement between two solutions for each value of the volume fraction exponent is found.

Table 3

Comparison of the normalized deflections of a simply supported FG plate (a/b = 1, a/h = 10) under ambient temperature for different values of volume fraction exponent between the developed finite element model and analytical approach [3].

Method	n = 0.5	n = 1.0	n = 5.0	n = 10
Analytical [3]	0.325	0.343	0.380	0.396
This work	0.3297	0.3515	0.3901	0.4050

Figure 4 shows the computed numerical results using the developed method in which the dimensionless deflections are expressed as a function of temperature for fully clamped FG plates fabricated by three different pairs of materials Al_2O_3/SUS304; Si_3N_4/SUS304 and ZrO_2/SUS304. The geometrical parameters of FG plates utilized for this analysis are set to be a/b = 1 and a/h =

10, and the conditions under which the plates being considered suffer high temperature environment, as the temperature interval is ranged from $T = 300K$ up to $1400K$. Notice that we limit our study to such a specified range of temperature, and any other values of temperature outside that interval are not considered either. It is naturally to understand the circumstance that under working conditions, in manufacturing or in-service for instance, the FG plates often operate in a certain environment in which the temperature bound is fully controlled.

The computed numerical results of the normalized deflections for thee FG plates depicted in Fig. 4 are very interesting as they reveal a significant impact of the temperature condition on the mechanical deflections. It is also found the same for the volume fraction exponent, which greatly alters the dimensionless deflections of FG plates. For the Al_2O_3/SUS304 and Si_3N_4/SUS304 plates, the normalized deflections get larger for the entire range of the temperature when increasing the volume fraction coefficient. More interestingly, under the same condition the pure metal plates deformed in such a way that their deflections are larger than those of the pure ceramic plate and any other FG plates whose properties are more and more ceramic. By suffering higher temperature conditions, the deflections induced by the pure metal plates even get larger as clearly seen in the picture. It may be due to the fact that once the pure metal plates placed in high temperature environment, the stiffness degradation of the plate is the main source that makes the deformation of plates larger. In the contrary, the mechanical behaviors of the ZrO_2/SUS304 plate are much more complicated than those of the other two FG plates. The pure SUS304 metal plate yields smaller deformations compared to the pure ZrO_2 ceramic plate at the temperature approximately $T = 1080K$, beyond that range of temperature up to $1400K$, the situation changes oppositely and the deformation of the pure SUS304 metal plate is the winner, meaning

that the SUS304 plate after the transition point yields larger deflections compared to the ZrO_2 ceramic one. This indicates a significant difference on the deflection behavior of ZrO_2/SUS304 plate as its response naturally generates a transition point, which does not appear to that of the Al_2O_3/SUS304 and Si_3N_4/SUS304 plates. A close-up view at the transition point of the deflection of the ZrO_2/SUS304 plate is also illustrated in the picture.

In overall, an increase of the dimensionless deflections can be found for all FG plates for the whole range of temperature. The metal SUS304 plates yield larger deformation than the Al_2O_3 and Si_3N_4 ceramic plates, however it depends on the temperature range whether the SUS304 plate can yield larger or smaller deformation compared to the pure ZrO_2 ceramic plate. As the FG plates become more and more metallic, the larger deflections are obtained as compared to those whose properties are more and more ceramic. The capability of withstanding large deformation in high temperature environment of the ceramic materials is shown, which are well known as a special material well sustaining high temperature conditions, are often designed to be working under such tough conditions of temperature.

While the normalized deflections obtained by the proposed model for the Al_2O_3/SUS304 and Si_3N_4/SUS304 plates are found to be almost similar between each other, opposite behaviors of the mechanical deflections of the ZrO_2/SUS304 plate compared to the Al_2O_3/SUS304 and Si_3N_4/SUS304 plates can be observed. It can be concluded that the mechanical bending behaviors of the FG plates are to be material-dependent, mainly caused by the nonlinear thermal properties and material behaviors of constituent materials. In other words, not all the FG plates in high temperature environment possess the same situation, they, as observed numerically, behave different from each other. Therefore, material combinations in terms of FGMs are important and

greatly affect the mechanical static bending behaviors of resultant FG plates and their performance under high temperature conditions. Consequently, this phenomenon and behaviors of FGMs may be important to the design and development of the FGMs in engineering applications, especially for those that suffer tough conditions of temperature. Such information might also be helpful to the designers or researchers in the appropriate selection of FGMs for specific purposes of utilizing the FGMs, for instance, a right selection of the FGMs to a right condition, e.g., structures to be working under high temperature conditions, is of course a great benefit in practice.

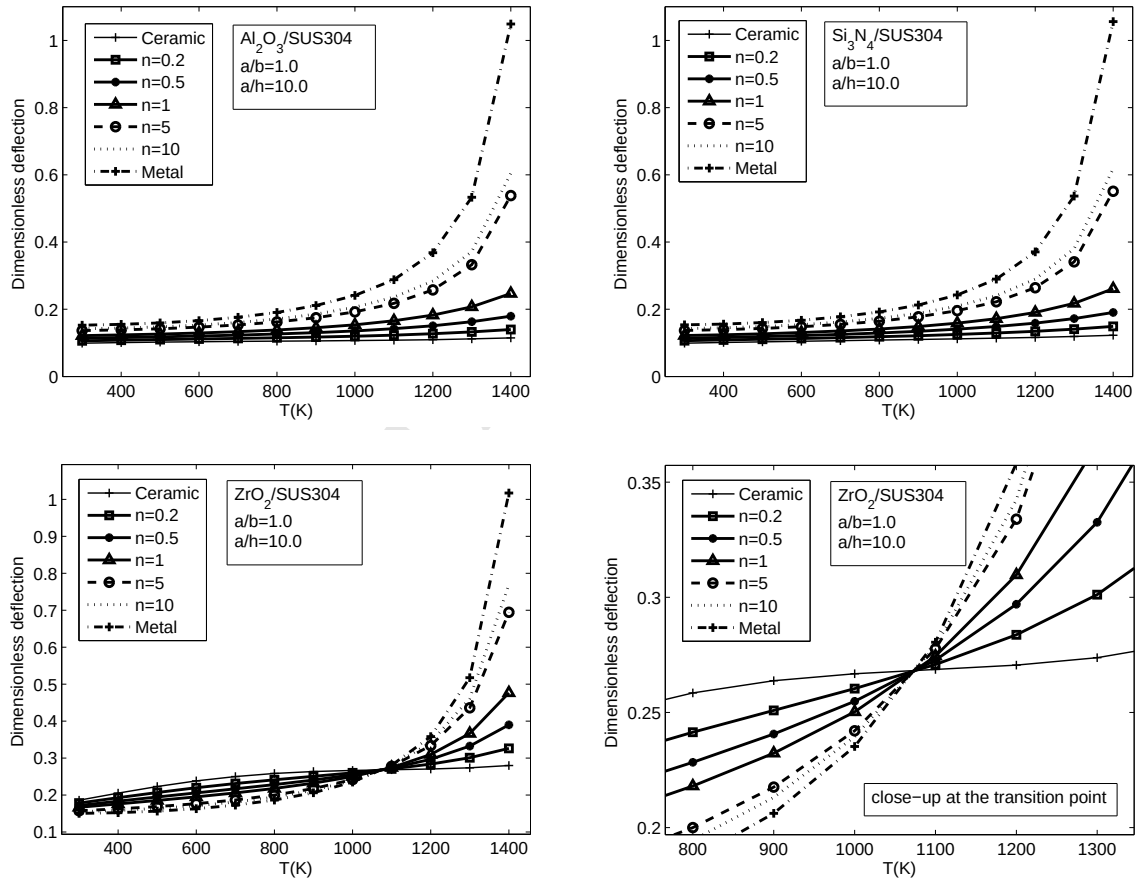

Fig. 4 Dimensionless deflections of fully clamped FG plates (a/b = 1, a/h = 10) made of Al_2O_3/SUS304 ; Si_3N_4/SUS304 and ZrO_2/SUS304 calculated by using the developed finite element model, showing the effects of volume fraction coefficient and temperature on the mechanical behaviors of FG plates.

To additionally explore the physical reason which leads to the difference on the mechanical behaviors of ZrO_2/SUS304 and those of the Al_2O_3/SUS304 and Si_3N_4/SUS304 plates, the Young's modulus and the coefficient of thermal expansion described in Eq. (2) as a function of temperature for each constituent material (i.e., SUS304, Al_2O_3, Si_3N_4 and ZrO_2) are hence depicted in Fig. 5, possessing a big difference on the behaviors among constituent materials. In Fig. 5, E_0 and α_0 are the reference values of E_{SUS304} and α_{SUS304} at $T_0 = 300K$ as given in Table 1. It is important to point out here that the material combinations, the nonlinear thermal properties and material behaviors of constituent materials are the main sources that make the mechanical behaviors of FGMs differently from each other. By looking at Fig. 5, it is very important to see that the transition on the behaviors of the Young's modulus can be found for the FG plate made of ZrO_2 and SUS304, whereas such transition behavior does not take place for other FG plates made of Al_2O_3 or Si_3N_4 combined with SUS304. Easily to see that the Young's modulus of ZrO_2 and SUS304 starts transitioning at a temperature approximately $T = 1080K$, which does not happen to the Al_2O_3 or Si_3N_4 and SUS304. Therefore, the material combinations and the behaviors of used constituent materials create a significant difference on the overall mechanical behaviors of FG plates.

Nevertheless, it is shown that the characteristics of the Young's modulus and the coefficient of thermal expansion of constituent materials greatly alter the overall behaviors of FGMs. Here, the matters happen to the ZrO_2 whose behavior is significantly different from that of the Al_2O_3 or Si_3N_4. We further show in Fig. 6, which is aimed at explicitly illustrating the variation behaviors of the Young's modulus and the coefficient of thermal expansion through-the-thickness of the Al_2O_3/SUS304 and ZrO_2/SUS304 plates (n = 0.5) affected by the temperature. It is very

interesting and one can thus observe a quite difference on the behaviors of the two considered plates, and more importantly, the transition behavior only occurs to the ZrO_2/SUS304 plate at a temperature approximately $T = 1080K$ as clearly exhibited in the picture. In fact, at the transition point, the non-homogeneous properties of FGMs degenerate to homogeneous by which the non-homogeneous FG plate becomes either homogeneous ceramic ZrO_2 or metal SUS304 plate irrespective of the volume fraction exponent effects.

Furthermore, we also observe that the characteristics of the metal SUS304 additionally alter the overall behaviors of FGMs. The stiffness of the metal SUS304 becomes softer in higher temperature as its Young's modulus decreases with respect to the temperature. Generally, under high temperature environments it apparently indicates a very important effect of the material combinations on the overall mechanical behaviors of FGMs, the obvious difference on the mechanical response of ZrO_2/SUS304, Al_2O_3/SUS304 and Si_3N_4/SUS304 plates shown in Fig. 4 is hence illustrated.

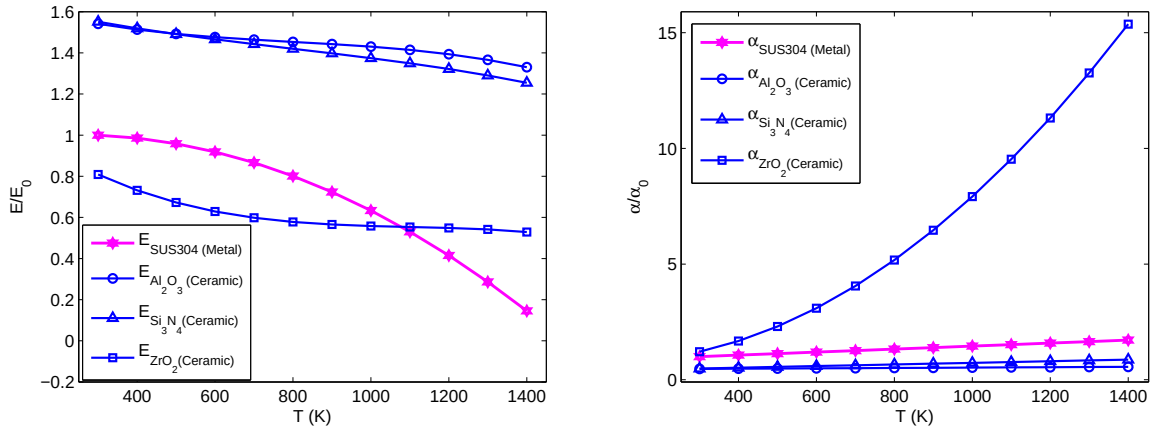

Fig. 5 Representative behaviors of the Young's modulus and the coefficient of thermal expansion as a function of temperature for each constituent material: SUS304, Al_2O_3, Si_3N_4 and ZrO_2. The material combination of ZrO_2 and SUS304, formed by ZrO_2/SUS304, naturally creates a transition point on its inherent mechanical behavior, which is found differently from that of Al_2O_3/SUS304 and Si_3N_4/SUS304.

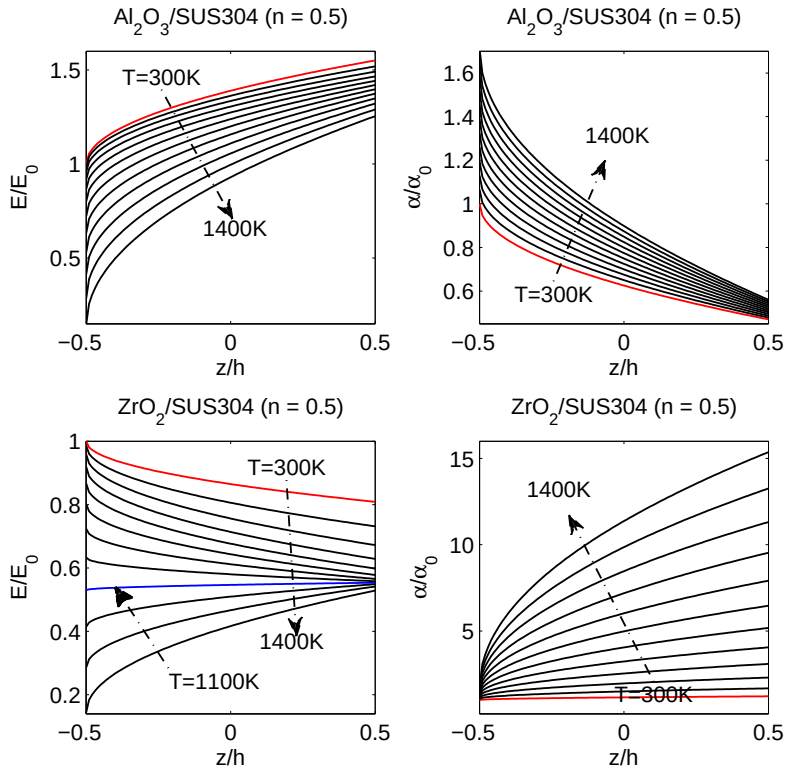

Fig. 6 Variation behaviors of the Young's modulus and the coefficient of thermal expansion through-the-thickness of Al_2O_3/SUS304 and ZrO_2/SUS304 plates (n = 0.5) affected by the temperature.

Next, we analyze the effect of the aspect ratio (*a/b*) of FG plates on the mechanical deflection using the proposed formulation. By accomplishing it, a rectangular FG plate made of Si_3N_4/SUS304 with *a/h*=10 is taken, sustaining in high temperature conditions from $T = 300K$ up to $800K$. Different values of the aspect ratio such as *a/b* = 0.2; 0.33; 1; 2 and 4 are considered. The volume fraction exponent of FG plates *n* = 1 is used for the analysis. The computed numerical results of dimensionless deflections are thus presented in Table 4 and also depicted in Fig. 7. As expected, a significant variation of the mechanical deflections of the FG plate over the aspect ratio (*a/b*) can be clearly observed. As a result, the influence of the ratio *a/b* on the dimensionless deflections of FG plates is high. However, the variation of the normalized deflections as a function of temperature is insignificant as it shows a slight increase of the deflection when the FG plate places in environment with higher temperature. It is worth noting that the characteristic of the sides *a* and *b* configuring the plate is different, which may be due to the fact that we keep the thickness-to-length *a/h*=10 unchanged throughout the analysis.

Table 4

Effect of the aspect ratio (*a/b*) on the dimensionless deflections of a rectangular FG Si_3N_4/SUS304 plate (*a/h* = 10) using the present formulation.

a/b	*T*=300*K*	400	500	600	700	800
0.2	0.2562	0.2608	0.2669	0.2746	0.2844	0.2968
0.33	0.2364	0.2407	0.2462	0.2533	0.2624	0.2739
1	0.1219	0.1242	0.1270	0.1306	0.1353	0.1412
2	0.0196	0.0199	0.0204	0.0210	0.0217	0.0226
4	0.0025	0.0026	0.0026	0.0027	0.0028	0.0029

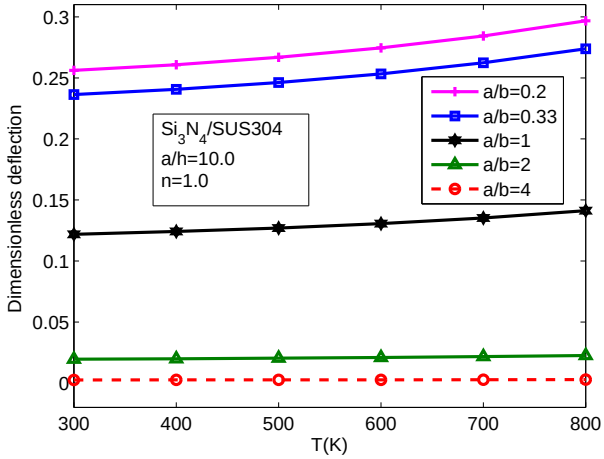

Fig. 7 Variation of the aspect ratio (*a/b*) and its effect on dimensionless deflections of a fully clamped FG plate (*a/h* = 10) made of Si_3N_4/SUS304 by the developed finite element model.

In order for exploring the effect of the thickness-to-length aspect ratio *a/h* on the mechanical bending response of FG plates in high temperature conditions, the normalization of the deflections is however redefined for this specific investigation, which, we expect to not take into account any effects caused by the thickness term as it presents in the previous formulation, Eq. (28). The new normalization for this specified analysis is hence formed as follows:

$$\overline{w} = \frac{w_c E_m}{1000\left(1-\nu_m^2\right) Pa} \tag{29}$$

The study is carried out and numerical experiments are performed over three square FG plates (*a/b* = 1) made of Al_2O_3/SUS304; Si_3N_4/SUS304 and ZrO_2/SUS304, respectively. The boundaries of the FG plates are fully clamped, while a constant temperature of $T = 800K$ is assumed throughout the analysis. The plates whose thickness are to be thin to moderate thick are considered as different values of the aspect ratio, e.g., *a/h* = 50; 30; 20; 10 and 5, are taken. The numerical results of the dimensionless deflections calculated by using the developed finite element formulation are then tabulated in Table 5 and also sketched in Fig. 8. The mechanical

deflections of three square FG plates are obtained for various values of volume fraction exponent including the pure metal and ceramic cases. Not surprisingly, by reducing the plate thickness the larger the mechanical deflections of FG plates is obtained, by which a great influence of the thickness-to-length aspect ratio (*a/h*) on the bending behaviors of the FG plates is exhibited. Furthermore, we have also found out that the dimensionless deflections increase with increasing the volume fraction coefficient, but this phenomenon takes place to the FG plates that are made of Al_2O_3/SUS304 and Si_3N_4/SUS304. Opposite situation however can be observed in such a way where the FG plate is made of ZrO_2/SUS304, increasing the volume fraction exponent leads to an decrease of the dimensionless deflections, by which one important point raised above that not all the FG plates behave the same situation can be confirmed. As a result, the mechanical response of FGMs under high temperature environment is to be material-dependent.

Our own numerical experiments have additionally found that the present formulation can avoid shear locking effect as it can be applied to solve thin plates successfully, as matrices of involving shear terms require only C^0 continuity. It must be stressed out here in this manuscript that the authors do not intend to repeat a comprehensive analysis of verifying the shear-locking effect of the used new TSDT as it was already studied and reported in the original work by Shi [6], curious readers may refer to [6] for more information. Therefore, we here focus our attention on presenting new numerical results and numerical investigations of the mechanical response of FG plates in high temperature environment.

We further explore the mechanical deflections as a function of temperature affected by the thickness-to-length aspect ratio (*a/h*). The present numerical results of this analysis are hence schematically sketched in Fig. 9, also experimenting over three fully clamped square FG plates

(a/b = 1) above. Only n = 0.5 which represents the volume fraction exponent of FG plate is considered. The numerical results obtained are very interesting as the thinner plates yield larger deflections than the thicker ones. The mechanical deflections of all FG plates increase for the higher range of temperature. It means that when the FG plates suffering higher temperature environments, larger deflections for all considered FG plates can be reached.

Table 5

Effect of the thickness-to-length aspect ratio (a/h) on the dimensionless deflections of fully clamped square FG plates (a/b = 1) using the present formulation.

			Al_2O_3/SUS304		
a/h	Ceramic	n=0.2	5.0	10	Metal
50	1.1033	1.2140	1.6838	1.7707	2.0001
30	0.2421	0.2671	0.3710	0.3902	0.4136
20	0.0735	0.0810	0.1129	0.1188	0.1334
10	0.0103	0.0114	0.0160	0.0169	0.0188
5	0.0018	0.0020	0.0029	0.0030	0.0033
			Si_3N_4/SUS304		
50	1.1409	1.2517	1.7135	1.7990	2.0211
30	0.2503	0.2745	0.3764	0.3952	0.4136
20	0.0760	0.0833	0.1145	0.1202	0.1347
10	0.0107	0.0116	0.0162	0.0171	0.0189
5	0.0019	0.0020	0.0029	0.0031	0.0033
			ZrO_2/SUS304		
50	2.6828	2.4999	2.0936	2.0330	1.9357
30	0.5894	0.5494	0.4596	0.4463	0.4136
20	0.1794	0.1673	0.1397	0.1357	0.1294
10	0.0255	0.0238	0.0197	0.0192	0.0184
5	0.0046	0.0043	0.0035	0.0034	0.0033

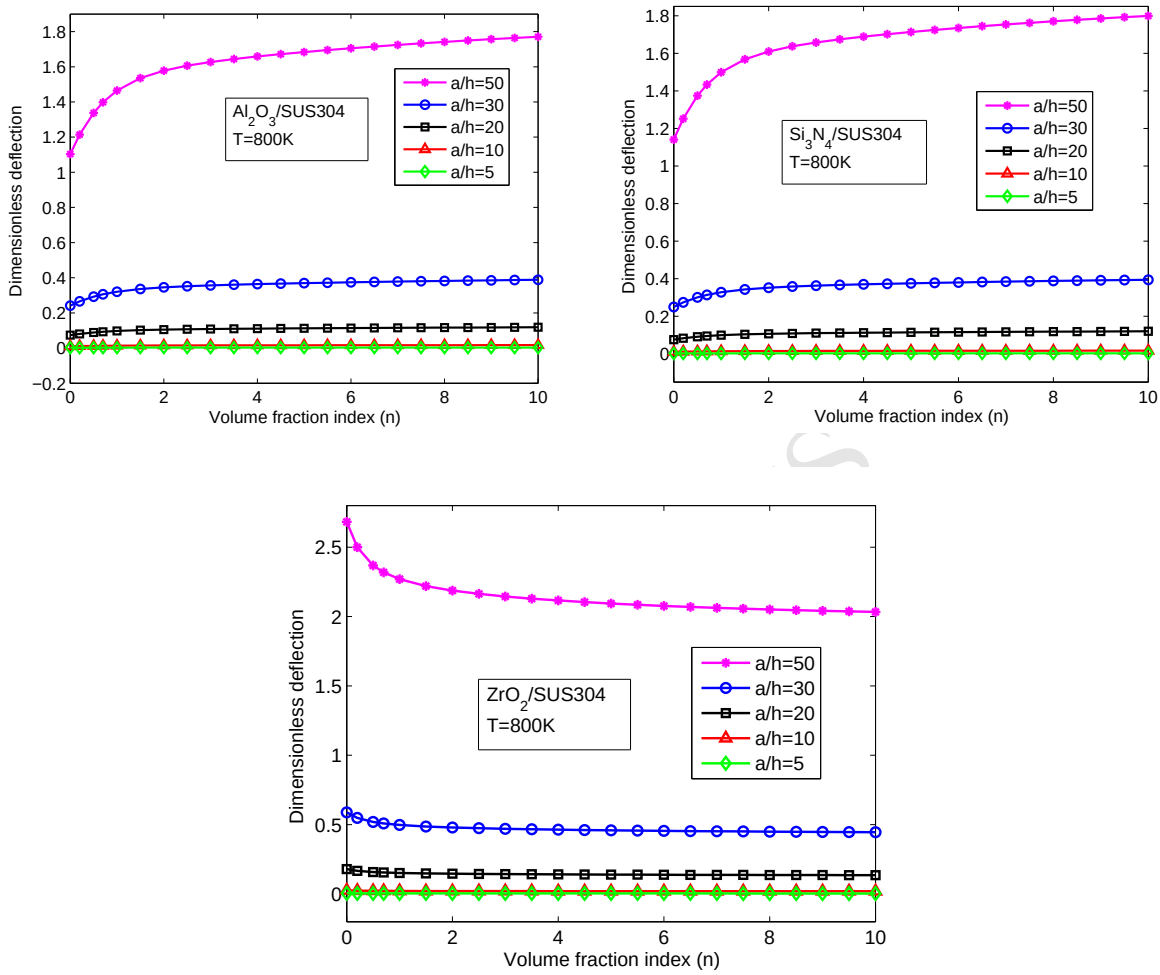

Fig. 8 Variation of the thickness-to-length aspect ratio (*a/h*) and its effect on dimensionless deflections of fully clamped square FG plates (*a/b* = 1) as a function of volume fraction exponent.

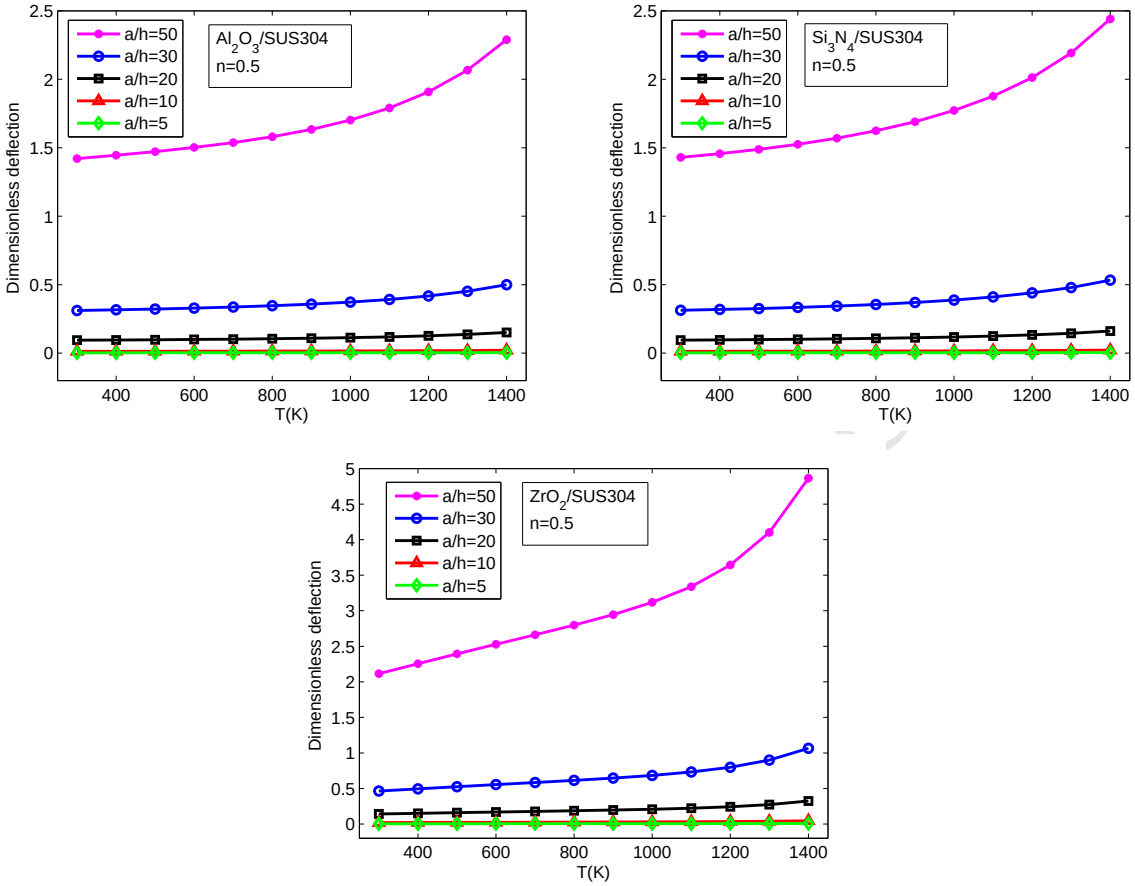

Fig. 9 Variation of the thickness-to-length aspect ratio (*a/h*) and its effect on dimensionless deflections of fully clamped square FG plates (*a/b* = 1) as a function of temperature.

The stress distributions in heated FG plates would be very interesting and they are now analyzed. We hence deal with a simply supported FG plate (*a/b* = 2) made of Si_3N_4/SUS304 suffering high temperature environments of $T = 800K$. The volume fraction index of FG plate *n* = 1 is indicated for this study of stress distributions. However, different values of the thickness-to-length ratio such as *a/h* = 5, 10 and 20 are examined. For simplicity and convenience in representation of the numerical results, the stresses at the middle point of plate obtained by the developed model are normalized by the following equations:

$$\{\bar{\sigma}_{xx};\bar{\sigma}_{yy};\bar{\sigma}_{xy};\bar{\tau}_{yz};\bar{\tau}_{xz}\}=\frac{h}{Pa}\{\sigma_{xx};\sigma_{yy};\sigma_{xy};\tau_{yz};\tau_{xz}\}(\frac{a}{2},\frac{b}{2},\frac{h}{2}) \quad (30)$$

Fig. 10 shows the through-the-thickness distributions of the stress components in the FG plate under uniform load for different thickness-to-length ratios. Clear distinction among the curves is obvious in the figures, revealing that the effect of the thickness-to-length ratios on the mechanical behaviors of the plate (stress distribution) is significant. The in-plane longitudinal and normal stresses (σ_{xx} and σ_{yy}) are first compressive and then tensile throughout the plate as exhibited in Fig. 10. One can also observe that the maximum values of the compressive and tensile stresses may occur on the bottom and top surfaces of FG plates. In addition, it is evident that the minimum value of zero for the σ_{xx} and σ_{yy} takes place at a point that is not the middle of plate due to the non-homogeneous properties of FG materials, as a result of asymmetry of the stress distributions in the FG plates. It can further be found from the stress distributions that the compressive and tensile values of the longitudinal tangential stress σ_{xy} at the middle point of plate are different from that of the σ_{xx} and σ_{yy}, their distributions are even more complicated. While the through-the-thickness distributions of the shear stresses τ_{yz} and τ_{xz} are fully different from other stresses, the shear stresses increase with decreasing the thickness-to-length ratio. Although the response of the shear stresses behaves in a similar situation, but the amplitude of the stress τ_{xz} is found to be smaller than the stress τ_{yz}. Nonetheless the maximum values of the stresses occur not at the plate center as often observed in the homogeneous plates. In all cases, one can conclude that the thickness-to-length ratio has a great impact on the mechanical behaviors of heated FG plates.

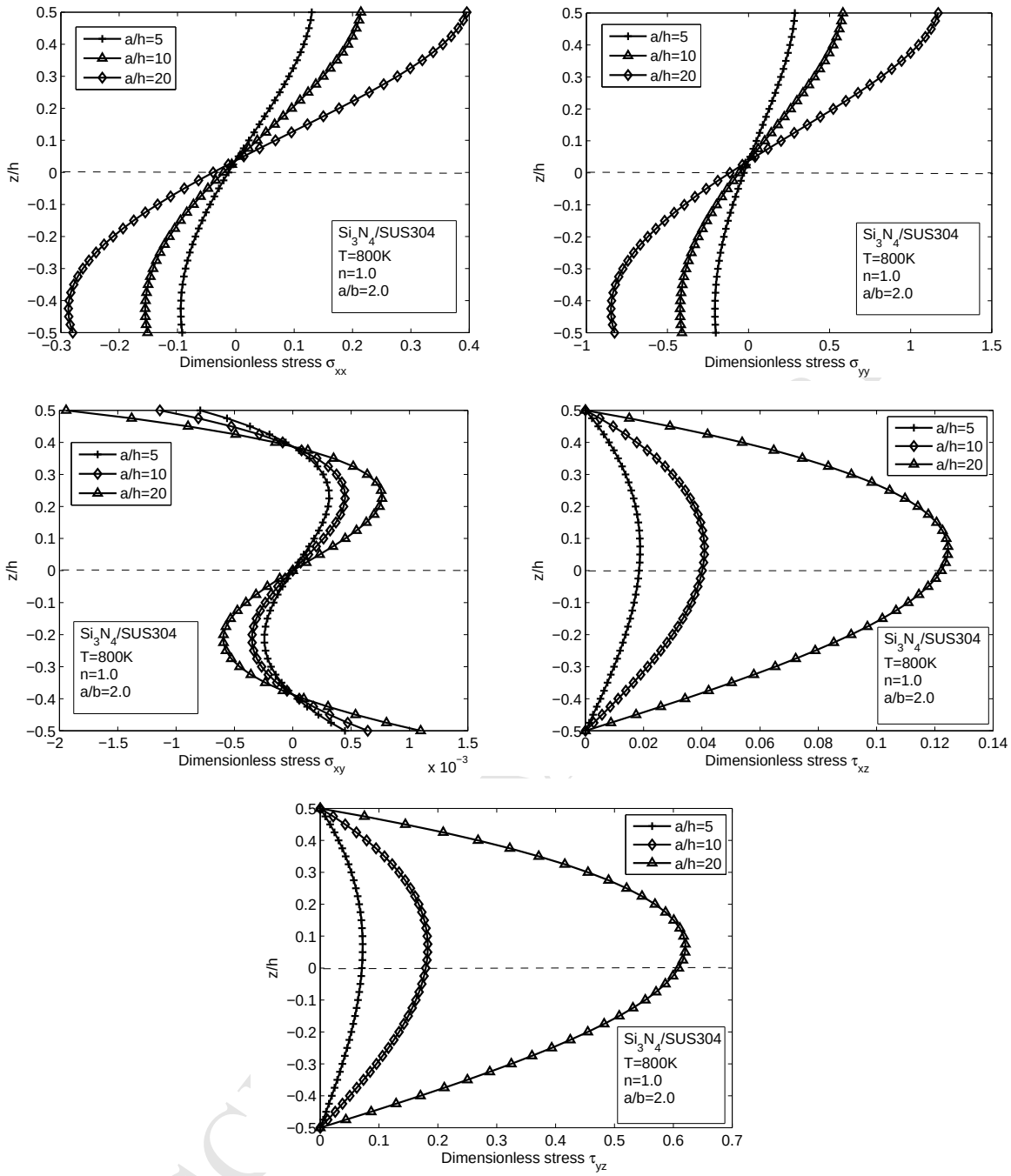

Fig. 10 Stress distributions through the thickness of an FG Si_3N_4/SUS304 plate (*a/b* = 2) for different values of thickness-to-length ratio obtained by the developed finite element model.

The effect of volume fraction exponent on the stresses distributed through-the-thickness in FG plates is also investigated numerically. The same simply supported FG plate made of Si_3N_4/SUS304 under condition of $T = 800K$ is considered, examining three different values of

gradient indices of FG plates such as n = 0.2, 1 and 10. Three individual tasks based on the developed finite element model for extracting the stresses are performed. The computed results of the in-plane longitudinal σ_{xx} shear τ_{yz} stresses are then depicted in Fig. 11. As exhibited in the figure that the volume fraction exponent greatly alters the stress distributions through-the-thickness in FG plates. In a similar manner, the influence of temperature on the stresses distributed through-the-thickness in FG plates is also explored. The computed stresses dependent upon the temperature are hence shown in Fig. 12 for three different values of temperature, $T = 300K$; $800K$ and $1400K$, respectively. The volume fraction exponent n = 0.2 is taken for this analysis. In overall, the stress distributions through-the-thickness in FG plates affected by temperature are insignificant except the maximum values of the compressive stress (σ_{xx}), which occur at the bottom surfaces of FG plates, are different from each other once increasing the temperature.

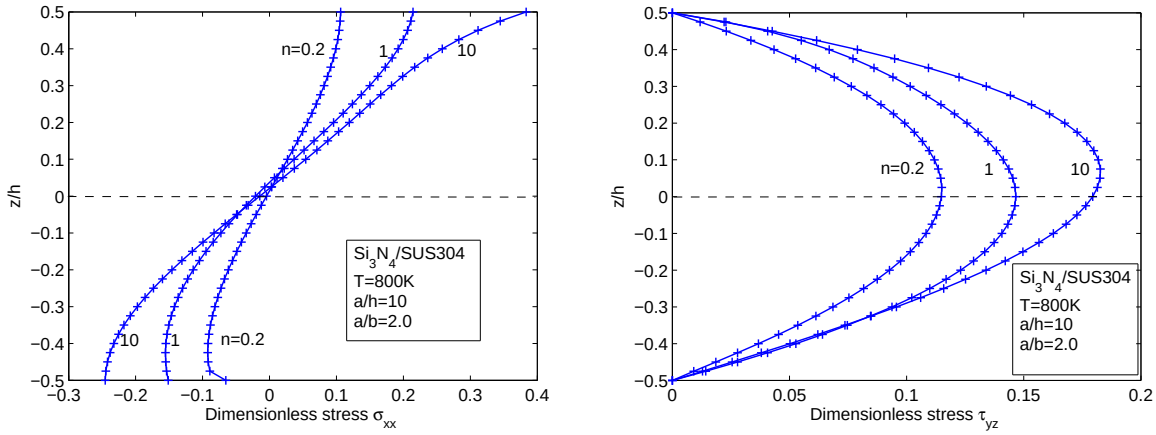

Fig. 11 Effect of volume fraction exponent on stresses (σ_{xx} and τ_{yz}) distributed through the thickness of an FG Si_3N_4/SUS304 plate (a/b = 2) obtained by the developed finite element model.

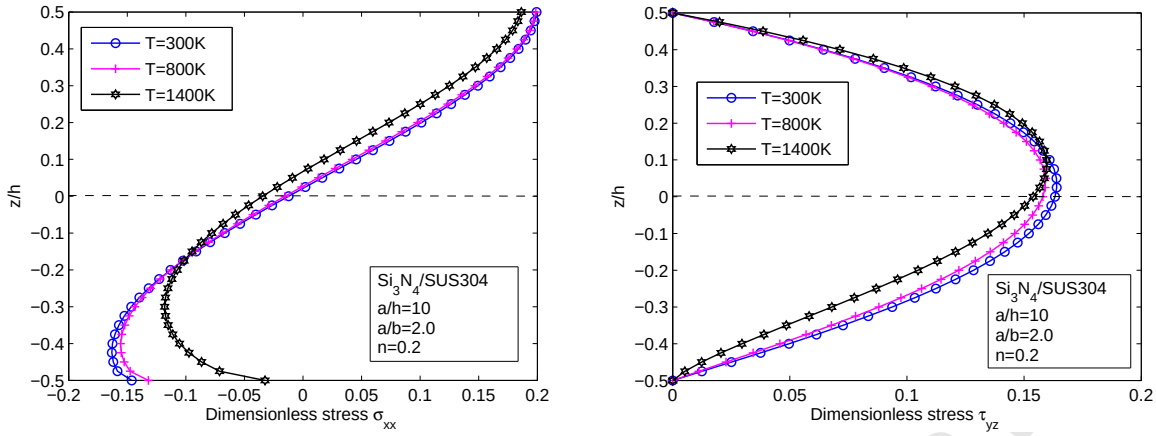

Fig. 12 Effect of temperature on stresses (σ_{xx} and τ_{yz}) distributed through the thickness of an FG Si_3N_4/SUS304 plate (a/b = 2) obtained by the developed finite element model.

4.1.2 A circle FG plate

The next example deals with a circle FG plate subjected to a uniform load P to further show the applicability of the proposed approach. The deflections of circle FG plates obtained by the present model are normalized by

$$\bar{w} = \frac{100 w_{\min} E_m h^3}{12\left(1-\nu_m^2\right) P R^4} \tag{31}$$

where R is a radius and h is the plate thickness. The developed finite element model is applied to solve this circle plate, and the mechanical deflections are then analyzed numerically. Similar to the previous example, three circle FG plates made of Al_2O_3/SUS304; Si_3N_4/SUS304 and ZrO_2/SUS304 are considered. In the numerical implementation, an aspect ratio of R/h = 10 is taken. Table 6 reports the dimensionless deflections of a fully clamped Al_2O_3/SUS304 plate as a function of temperature taken from $T = 300K$ up to $800K$, affected by the volume fraction exponents. The higher the volume fraction coefficient is taken the larger dimensionless deflections are obtained, revealing a significant variation of the mechanical response of FG

plates caused by the gradient index. In a similar manner, the higher the temperature is taken, the larger the deflections is gained, but the variation of the mechanical behavior caused by the temperature change is small for the plates whose properties are more and more ceramic, otherwise the variation becomes significant for those that properties approach to the metallic. This investigation is also visualized in Fig. 13, which additionally involves the results of pure metal plate and of Si_3N_4/SUS304 and ZrO_2/SUS304. Nonetheless, Fig. 14 shows the numerical results of the dimensionless deflections as a function of temperature up to $T = 1400K$ of Al_2O_3/SUS304, Si_3N_4/SUS304 and ZrO_2/SUS304 plates, computed by the developed finite element model. These results of circle FG plates are fully consistent with the previous examples. Unlike the Al_2O_3/SUS304 and Si_3N_4/SUS304 plates, the mechanical behavior of circle ZrO_2/SUS304 plate in high temperature is also found to be transitioned at a point where the temperature takes place approximately $T = 1080K$. Larger deflections can be gained for the pure metal plates on the condition that the plates must be placed in higher temperature, e.g., $T = 1400K$. It may be due to the stiffness degradation of plates in high temperature, the material properties of metal become softer compared to the ceramic. Once again, the mechanical behaviors of deflections depicted in Fig. 14 are similar to that for square FG plates plotted in Fig. 4 above, confirming one important issue that not all the FG plates suffering high temperature environment deliver the same situation, they behave different from each other. As already investigated above, the material combinations, the behaviors and the nonlinear thermoelastic properties of constituent materials are those that make the mechanical behaviors of FGMs in high temperature differently as illustrated in Figs. 5 and 6.

Table 6

Dimensionless deflections of a fully clamped circle FG plate (R/h = 10) formed by Al_2O_3/SUS304 computed by the present formulation for different values of volume fraction exponent.

n	T=300K	400	500	600	700	800
0	1.3984	1.4240	1.4441	1.4597	1.4721	1.4830
0.2	1.5025	1.5294	1.5539	1.5776	1.6019	1.6285
0.5	1.6130	1.6409	1.6709	1.7048	1.7446	1.7928
1	1.7219	1.7506	1.7867	1.8323	1.8906	1.9658
5	1.9151	1.9453	1.9922	2.0592	2.1515	2.2774
10	1.9896	2.0204	2.0715	2.1466	2.2516	2.3961

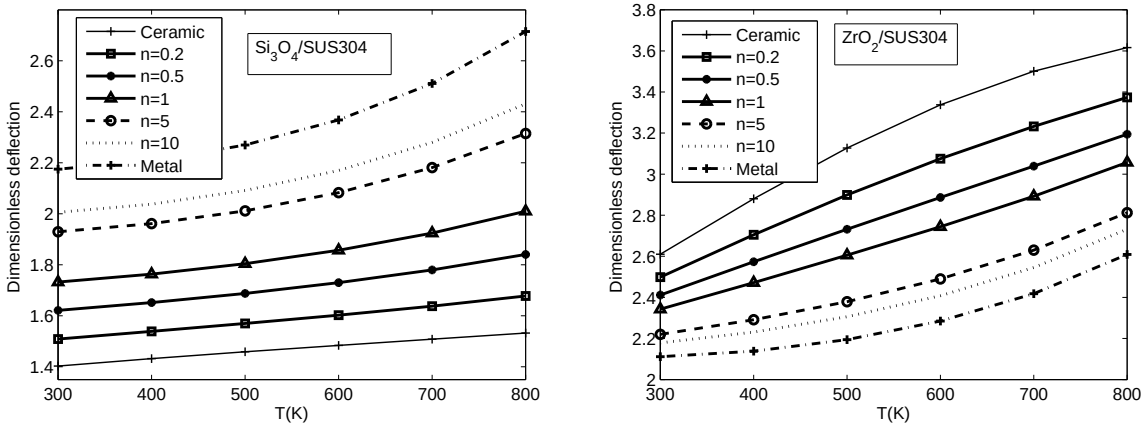

Fig. 13 Dimensionless deflections of fully clamped circle FG plates (R/h = 10) made of Si_3N_4/SUS304 and ZrO_2/SUS304 calculated by using the developed finite element model, showing the effects of volume fraction coefficient and temperature.

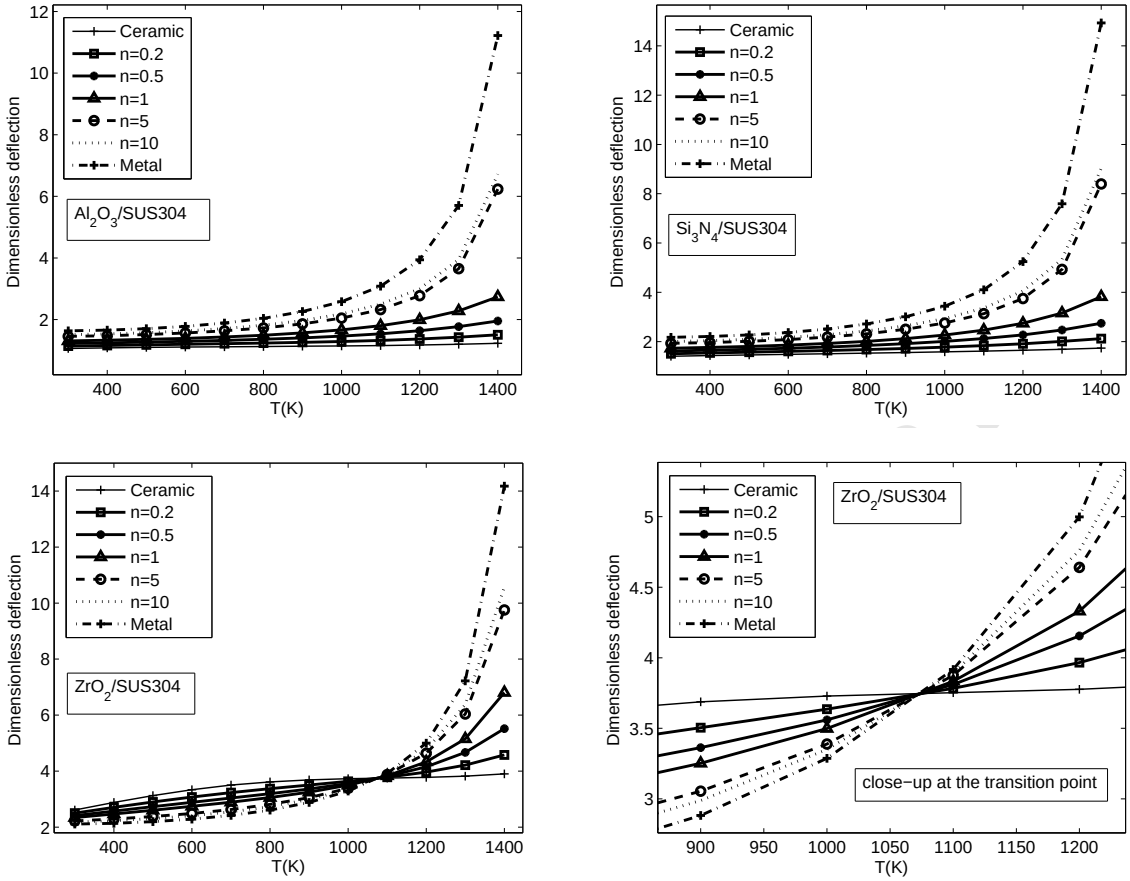

Fig. 14 Dimensionless deflections of two fully clamped circle FG plates (*R/h* = 10) made of Si_3N_4/SUS304 and ZrO_2/SUS304 calculated by using the developed finite element model, showing the effects of volume fraction coefficient and a wider range of temperature. The mechanical behaviors of the Si_3N_4/SUS304 plate are different from that of the ZrO_2/SUS304 plate. The numerical results of the dimensionless deflections of the ZrO_2/SUS304 plate are found the same as that for square FG plate above, they first increase and then decrease with increasing the volume fraction exponent and the transition point occurs at appropriately $T = 1100K$, and beyond that range, the deflections behave opposite.

The influence of the thickness-to-length aspect ratio (*R/h*) on the mechanical deflections of this circle FG plate is analyzed. For this particular example, we also redefine the normalization of deflections as follows:

$$\overline{w} = \frac{w_{\min} E_m}{1000\left(1-v_m^2\right) PR} \tag{32}$$

Only a fully clamped Al_2O_3/SUS304 plate with different values of thickness-to-length aspect ratio *R/h* is analyzed. The dimensionless deflections as a function of thickness-to-length ratio altered by the volume fraction exponent are depicted in Fig. 15 for $T = 300K$ and $1100K$, respectively. By specifying *R/h* = 20, 15, 10 and 5, thin and moderate thick plates are hence involved, interpreting the applicability of the developed formulation in solving thin plates without any effects of shear-locking. Once again, the dimensionless deflections increase with decreasing the plate thickness, showing a significant effect of the thickness-to-length ratio on the dimensionless deflections of FG plates. In other words, the thinner plates yield larger deflections than the thicker ones as usual. Additionally, the SUS304 metal plate also yields larger deflections compared to the Al_2O_3 and other FG plates whose properties are more and more ceramic.

Moreover, the non-dimensional deflection as a function of temperature of three Al_2O_3/SUS304; Si_3N_4/SUS304 and ZrO_2/SUS304 plates is also plotted in Fig. 16 for a volume fraction exponent of *n* = 0.5. These results aim to further interpret the variation of the mechanical behaviors of FG plates in high temperature environment affected by the thickness-to-length aspect ratio (*R/h*), and to confirm the physical phenomenon addressed in the previous square FG plates. It is again found that the thinner plates always yield larger values of the deflections, precisely showing a great influence of the thickness-to-length ratio on the mechanical behaviors of FG plates. Under higher temperature, the FG plates deform largely. It hence indicates a consistence of these numerical results obtained for circle FG plates with those of the previous example of square FG plates. Additionally, the deformation of a circle FG plate is also visualized in Fig. 17.

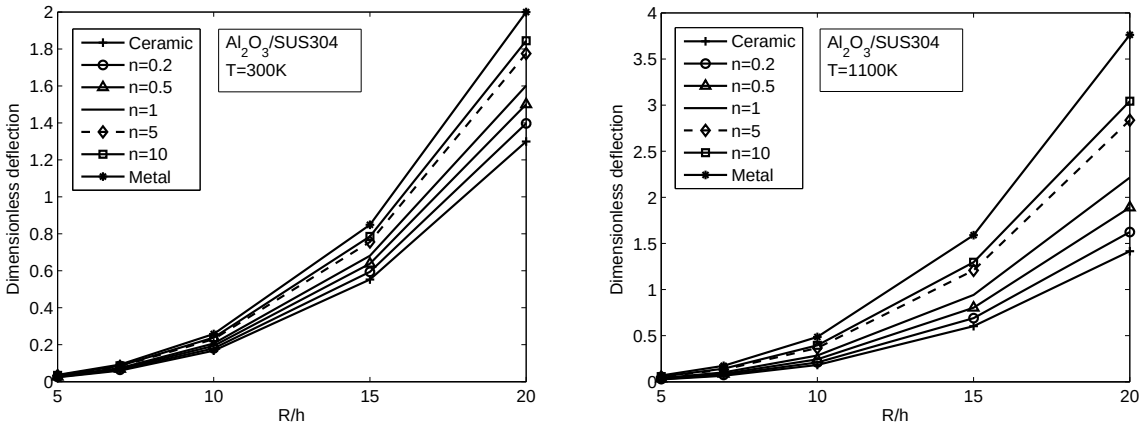

Fig. 15 Effect of the thickness-to-length aspect ratio (*R/h*) on the mechanical deflections of a fully clamped Al_2O_3/SUS304 plate for $T = 300K$ and $1100K$, respectively.

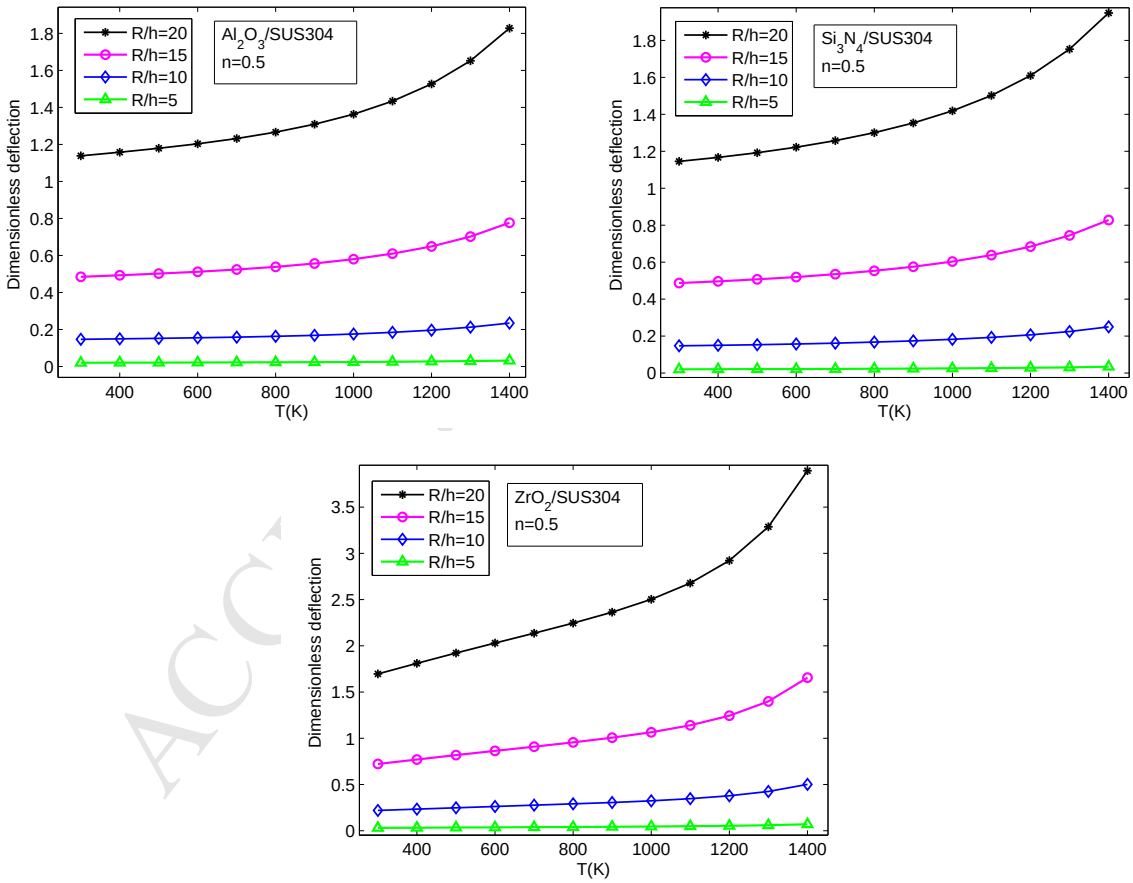

Fig. 16 Variation of the thickness-to-length aspect ratio (*R/h*) and its effect on dimensionless deflections of fully clamped circle FG plates as a function of temperature.

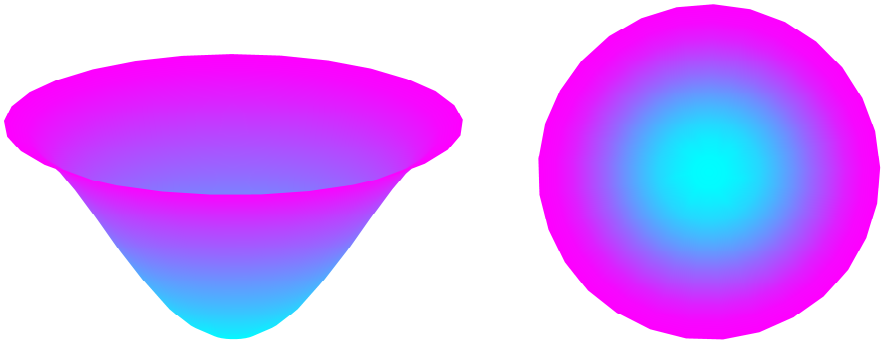

Fig. 17 Visualization of the mechanical deformation of a fully clamped circle heated FG plate under high temperature obtained by the proposed FE model, a front view (left) and a top view (right). A magnification factor of 100 is used to scale the picture.

4.1.3 A L-shape FG plate

The last example for static bending analysis devotes to a more complicated shape, an FG L-shape as its geometrical information is schematically sketched in Fig. 18. The plate is subjected to a uniform load P. Similarly, the deflections of the L-shape FG plate computed by the present finite element model are normalized by

$$\overline{w} = \frac{100 w_{\min} E_m h^3}{12\left(1-\nu_m^2\right) P L^4} \tag{33}$$

where L and b denote the sides of plate and h is also the plate thickness. The geometrical parameters of plate used for the analysis are set to be $L = b = 1$m, $L' = L/2$, $b' = b/2$, and $h = 0.025$m. Fig. 19 depicts the numerical results of the non-dimensional deflections as a function of the volume fraction exponent altered by the temperature varying from $T = 300K$ to $1400K$ for two fully clamped L-shape FG plates, e.g., Al_2O_3/SUS304 and ZrO_2/SUS304, respectively. As expected, the present numerical results reveal a significant influence of the volume fraction coefficient on the mechanical response. The difference on the mechanical behaviors between the Al_2O_3/SUS304 plate and the ZrO_2/SUS304 plate is obvious. The dimensionless deflections of the

Al_2O_3/SUS304 plate increase with increasing the volume fraction exponent, whereas those of the ZrO_2/SUS304 plate are found to be a little more complicated. It is, the transition point for the ZrO_2/SUS304 plate is again found at $T = 1080K$ approximately, quite similar to the previous examples. Under high temperature conditions, for instance, less than $T = 1080K$, the dimensionless deflections of the ZrO_2/SUS304 plate decrease with an increase of the volume fraction index, but beyond that range of temperature, i.e., $T \geq 1080K$, the larger the volume fraction exponent is taken the higher the deflections is obtained.

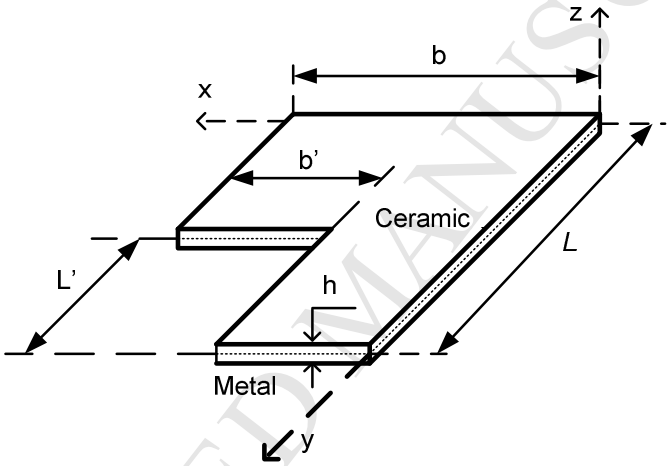

Fig. 18 Geometrical notation of a L-shape FG plate.

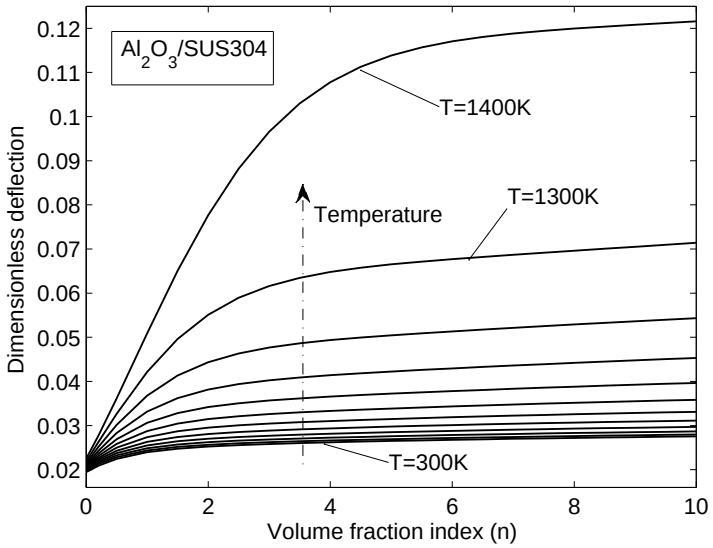

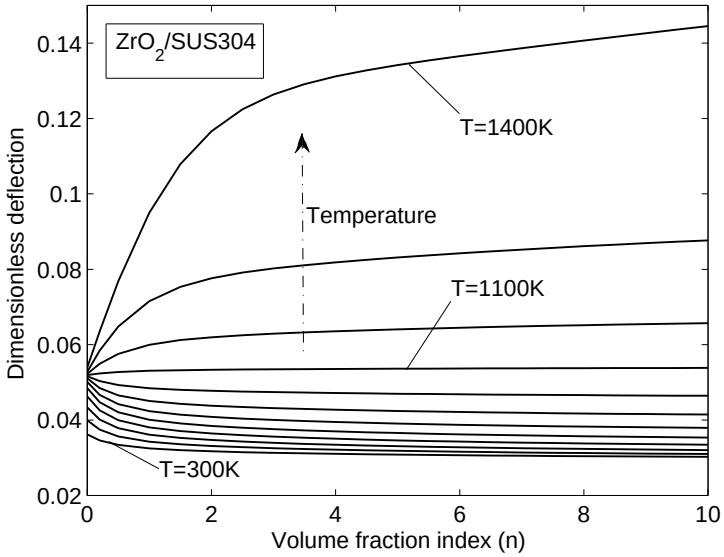

Fig. 19 Dimensionless deflections of two fully clamped L-shape FG plates made of Al_2O_3/SUS304 and ZrO_2/SUS304 as a function of volume faction exponent altered by temperature.

The boundary conditions affected the mechanical behaviors of FG plates in high temperature environments are now investigated numerically. We restrict our study by considering only the fully clamped (CCCC) and simply supported (SSSS) boundary conditions to an FG L-shape plate. A L-shape plate (b = 1m, L/b = 2) made of ZrO_2/SUS304 is considered are, three typical values of volume fraction exponent n = 0.1, 1 and 5 are considered, and the dimensionless deflections as a function of temperature for each value of volume fraction index are hence depicted in Fig. 20, highlighting the difference on the mechanical response caused by the boundary conditions. Very interesting results are gained as they show a great impact of the boundary conditions on the mechanical deflections of L-shape FG plates. The plate constrained by SSSS boundary condition yields larger deformations than that of CCCC. The results are quite reasonable because the SSSS inherently offers a more flexible boundary conditions than the CCCC.

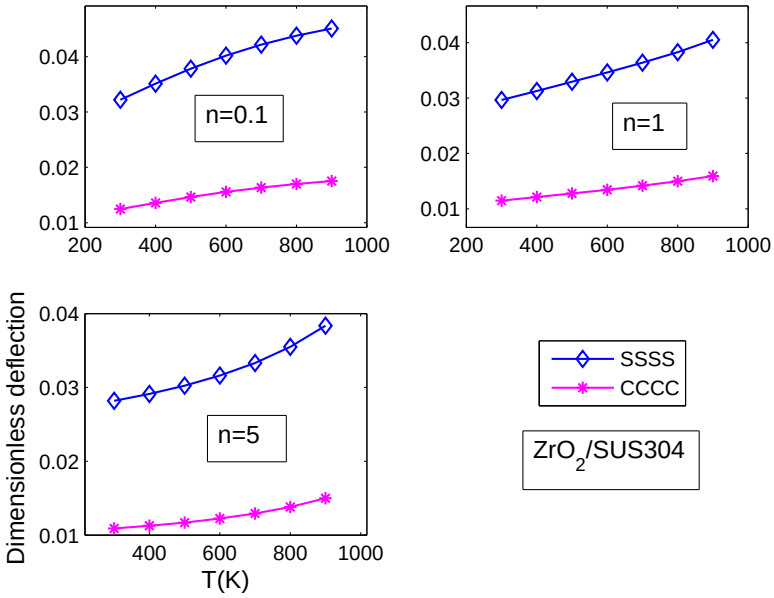

Fig. 20 Effect of boundary conditions on dimensionless deflections of L-shape FG plates (b = 1m, L/b = 2, h = 0.025m) made of ZrO_2/SUS304 as a function of temperature altered by volume faction exponent.

4.2 Numerical results for eigenvalue analysis

In this section, we numerically study the natural frequency of FG plates in high temperature environment utilizing the proposed finite element formulation. Similar to the static bending analysis, the rectangular, circle and L-shape plates are again used for the eigenvalue analysis.

4.2.1 A rectangular FG plate

We now investigate the free vibration of FG plates made of Al_2O_3/SUS304, Si_3N_4/SUS304 and ZrO_2/SUS304 under fully simply supported boundary conditions with different values of volume fraction index using the present formulation. We first verify the accuracy of the proposed finite model, the geometrical parameters of plate are set to be, such as length a = b = 0.2m, thickness h = 0.025m [3, 4], a square plate. The analytical solutions of natural frequency of this example available in [3, 4] are thus used for comparison purpose. The natural frequency results presented in the dimensionless frequencies are normalized by $\Omega = \left(\omega a^2 / h\right)\left[\rho_0 (1-\nu^2)/E_0\right]^{1/2}$,

where E_0 and ρ_0 are the reference values of E_m and ρ_m at $T_0 = 300K$ as given in Table 1. Table 7 presents a comparison of the first three modes of dimensionless natural frequencies of Al_2O_3/SUS304, Si_3N_4/SUS304 and ZrO_2/SUS304 square plates for different values of volume fraction exponent n = 0, 0.5, 1 and 2 among the present formulation and other two analytical solutions [3, 4]. As expected, the present numerical results reveal good agreements with reference exact solutions [3, 4], precisely confirming the accuracy of the present formulation in solving eigenvalue problems of FG plates.

In order to further validate the accuracy of the proposed method in high temperature, Table 8 thus presents a comparison of the fundamental frequency at high temperature (e.g., T= 400K, 500K and 600K) of two fully clamped Al_2O_3/SUS304 and Si_3N_4/SUS304 plates for different volume fraction exponents (e.g., n = 0.5, 1 and 5) between the proposed method and analytical method [3]. It is found that the frequencies at high temperature obtained by the present method are in good agreement with the analytical solutions [3]. The obtained numerical results are interesting as it indicates that the frequencies decrease with increasing the temperature. The frequencies also decrease when the material behavior of plates is more and more metallic. The Si_3N_4/SUS304 plates provide lower frequency results than those of the Al_2O_3/SUS304 ones.

Table 7

Comparison of the first three modes of dimensionless natural frequencies $\left(\Omega=\left(\omega a^2/h\right)\left[\rho_0(1-\nu^2)/E_0\right]^{1/2}\right)$ of simply supported FG square plates under ambient temperature (T=300K) (a = b = 0.2m, h = 0.025m) among the present formulation and other two exact solutions [3, 4]

mode	n = 0			0.5			1			2		
	Si_3N_4/SUS304											
	*	[3]	[4]	*	[3]	[4]	*	[3]	[4]	*	[3]	[4]
1	12.498	12.507	12.495	8.554	8.646	8.675	7.487	7.599	7.555	6.7052	6.825	6.777
2	29.301	29.256	29.131	20.559	20.080	20.262	17.987	17.705	17.649	16.083	15.947	15.809
3	45.061	44.323	43.845	31.088	29.908	30.359	27.209	26.727	26.606	24.326	24.147	23.806
	Al_2O_3/SUS304											
1	9.713	9.841	-	7.805	7.803	-	6.9974	7.114	-	6.5193	6.563	-
2	23.009	23.008	-	19.003	18.253	-	16.518	16.633	-	15.833	15.323	-
3	35.367	34.794	-	28.018	27.569	-	25.433	24.700	-	23.346	23.048	-
	ZrO_2/SUS304											
1	7.314	7.260	-	6.406	6.368	-	6.0747	6.037	-	5.796	5.753	-
2	17.101	16.953	-	15.119	14.824	-	14.544	14.014	-	13.898	13.294	-
3	25.959	25.671	-	24.719	24.570	-	21.582	21.456	-	20.636	20.247	-

* This work

Table 8

Dimentionless frequencies $\left(\Omega=\left(\omega a^2/h\right)\left[\rho_0(1-\nu^2)/E_0\right]^{1/2}\right)$ of fully clamped FG plates in high temperature (a/b = 1, a/h = 10) (E_0 and ρ_0 are the reference values of E_m and ρ_m at T_0 = 300K)

n	Method	Si_3N_4/SUS304			Al_2O_3/SUS304		
		T=400K	500K	600K	T=400K	500K	600K
0.5	[3]	15.938	15.468	14.939	14.384	14.003	13.592
	Present	15.355	15.192	15.008	13.484	13.724	13.589
1	[3]	13.915	13.462	12.941	13.025	12.631	12.188
	Present	13.433	13.280	13.093	12.566	12.440	12.287
5	[3]	11.175	10.749	10.242	10.965	10.556	10.073
	Present	10.852	10.716	10.528	10.645	10.520	10.343

Fig. 21 shows the dimensionless frequencies of the first mode as a function of temperature of fully clamped FG square plates made of Al_2O_3/SUS304, Si_3N_4/SUS304 and ZrO_2/SUS304 altered by the volume fraction exponent. It is evident that largest natural frequency is found for the pure ceramic plates. The natural frequencies decrease as the plates become more and more metallic. Interestingly, unlike the static bending results, the free vibration analysis of FG plates in high temperature environment delivers us a similar behavior on the natural frequencies regardless of any combinations of FGMs, i.e., all three considered FG plates made of Al_2O_3/SUS304, Si_3N_4/SUS304 and ZrO_2/SUS304 show similar behaviors on the natural frequencies. Globally, the overall behaviors of natural frequencies can be said similarly for all three FG plates as the normalized natural frequencies decrease with the temperature. However, by more carefully looking at the natural frequencies, one may find out that the ZrO_2/SUS304 plate causes differently in its natural frequency compared to that of two other FGMs, the Al_2O_3/SUS304 and Si_3N_4/SUS304. In any cases, the effect of the volume fraction exponent on the dimensionless frequencies of FG plates in high temperature conditions is significant.

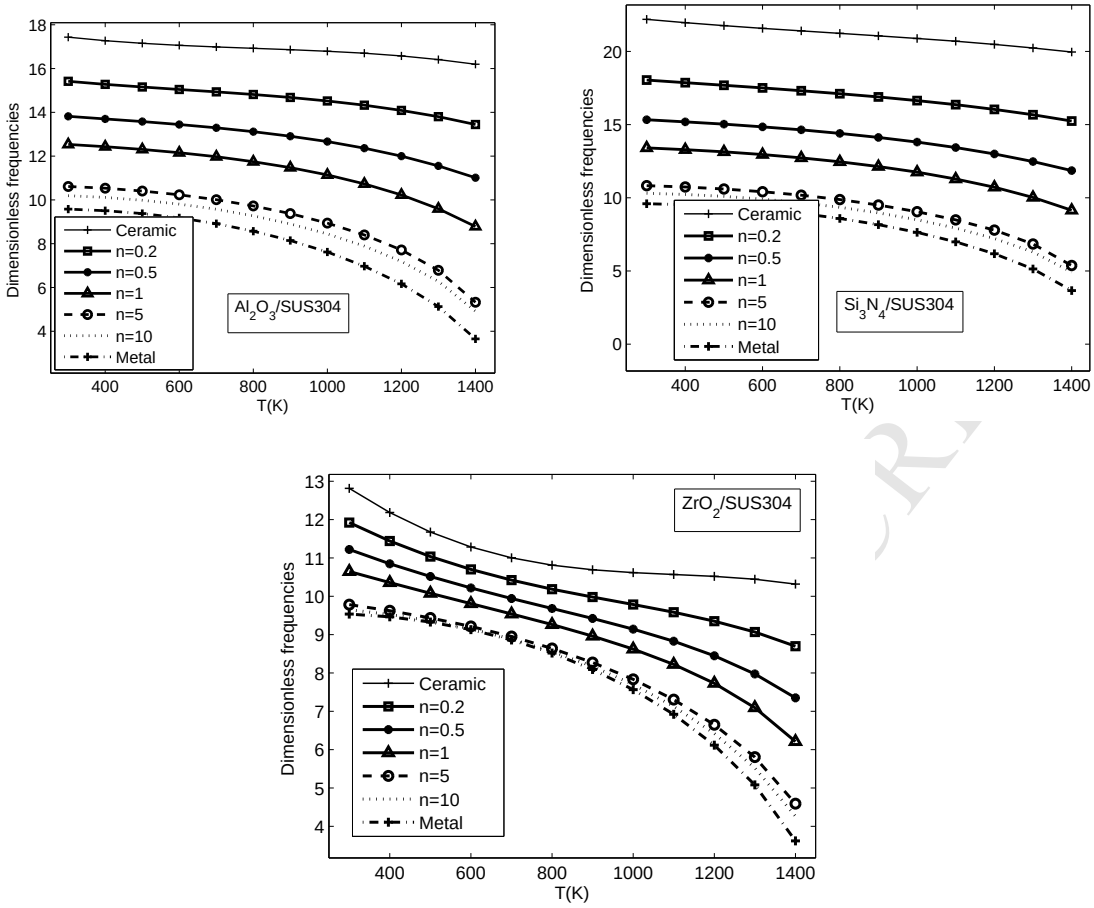

Fig. 21 Dimensionless frequencies as a function of temperature of fully clamped FGM plates (*a/b* = 1, *h* = a/10) made of Al_2O_3/SUS304, Si_3N_4/SUS304 and ZrO_2/SUS304

The thickness-to-length aspect ratio may have some effects on natural frequency of FG plates in high temperature. Three fully clamped FG square plates (*a/b* = 1) made of Al_2O_3/SUS304, Si_3N_4/SUS304 and ZrO_2/SUS304 are used for this analysis, and they are considered under a high temperature environment with $T = 800K$ for instance. Different thickness-to-length ratios such as *a/h* = 5, 10, 15, and 20 are examined. The dimensionless natural frequencies as a function of volume fraction exponent computed by utilizing the developed finite element are then shown in Fig. 22, and tabulated in Table 9. Very interesting results can be observed from the figures as all the FG plates deliver the same behavior, the dimensionless frequencies gradually decrease with

increasing the volume fraction exponent. The thicker plates induce lower natural frequencies compared to the thinner ones. The present numerical results clearly show a great variation of the natural frequencies caused by the thickness-to-length aspect ratio. In a similar circumstance, yielding higher natural frequencies is obtained for the Al_2O_3/SUS304 and Si_3N_4/SUS304 plates as compared to that of the ZrO_2/SUS304 plate.

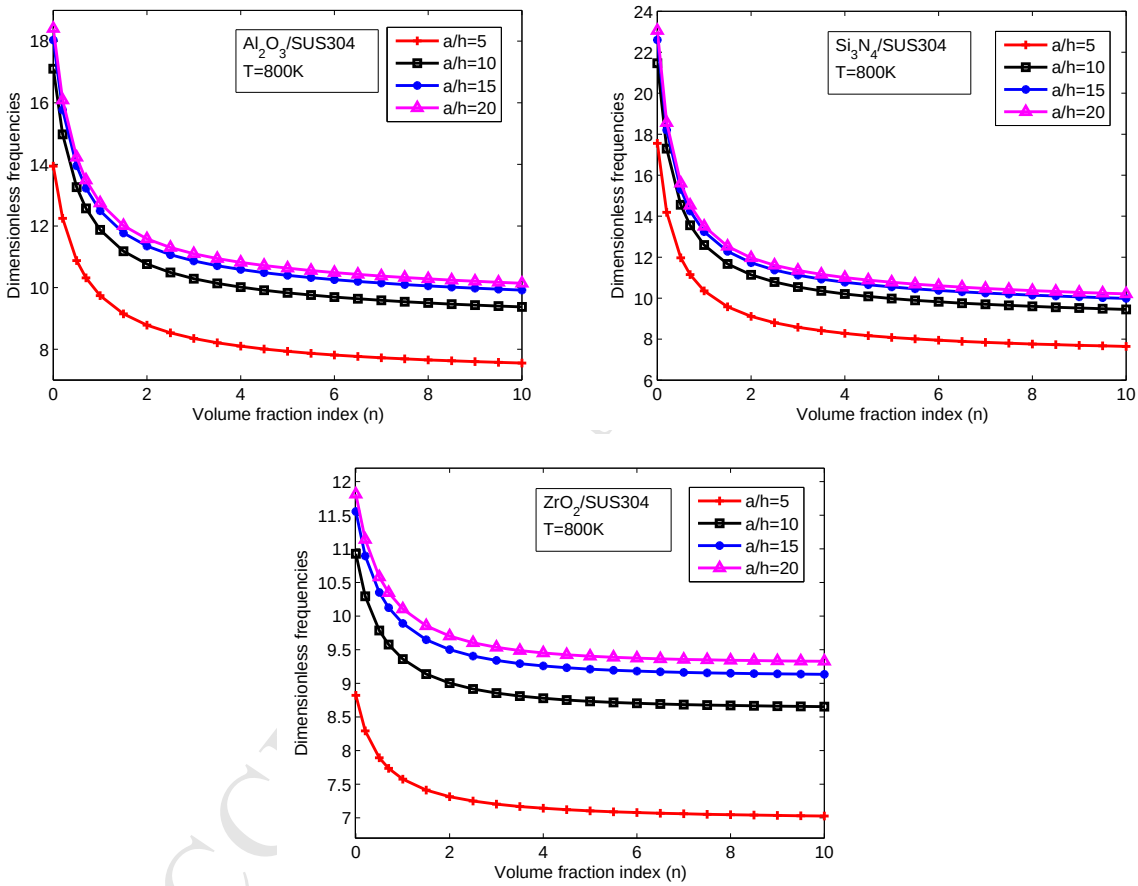

Fig. 22 Effect of thickness-to-length aspect ratio on dimensionless frequencies of fully clamped FGM plates (a/b = 1) made of Al_2O_3/SUS304, Si_3N_4/SUS304 and ZrO_2/SUS304.

Table 9

Numerical results of the effect of thickness-to-length aspect ratio on dimensionless frequencies of fully clamped FG plates (a/b = 1) made of Si_3N_4/SUS304 and ZrO_2/SUS304 obtained by the present method.

a/h	n =0	0.2	0.5	1	5	10
			ZrO2,800			
5	8.7567	8.2331	7.8357	7.5197	7.0514	6.9748
10	10.8115	10.1857	9.6822	9.2613	8.6400	8.5622
15	11.4209	10.7675	10.2308	9.7750	9.1032	9.0268
20	11.6679	11.0038	10.4533	9.9828	9.2897	9.2143
			Si3N4,800			
5	17.4159	14.0803	11.8767	10.2749	8.0247	7.5902
10	21.2296	17.1119	14.4005	12.4589	9.8772	9.3525
15	22.3327	17.9852	15.1249	13.0860	10.4231	9.8725
20	22.7758	18.3354	15.4151	13.3373	10.6443	10.0835

.

Next, we explore the influence of the boundary conditions on the dimensionless frequencies of FG plates in high temperature environment using the developed finite element model. We adopt the ZrO_2/SUS304 plate, which suffers $T = 800K$, and the numerical results of the dimensionless frequencies as a function of volume fraction exponent for different values of thickness-to-length aspect ratio are then plotted in Fig. 23. Different from the static bending results, the boundary conditions affect the natural frequencies oppositely, meaning that the FG plates constrained by CCCC boundary condition induce higher natural frequencies compared to that of SSSS. Once again, it is found that the thickness-to-length ratio greatly alters the frequencies. In addition, the dimensionless frequencies decrease as the plates become more and more metallic.

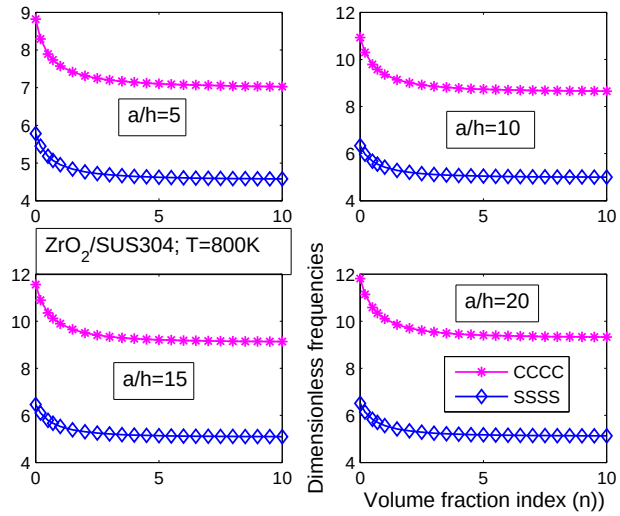

Fig. 23 Effect of boundary conditions on the dimensionless natural frequencies of an FG plate (*a/b* = 1) made of ZrO2/SUS304 altered by the thickness-to-length aspect ratio (*a/h*).

Similarly, Table 10 reports the first five modes of dimensionless frequencies of simply supported FG rectangular plates made of ZrO_2/SUS304 in high temperature condition, e.g., $T = 800K$, devoted to the analysis of the aspect ratio (*a/b*) on the natural frequencies. Numerical results are obtained in which different values of the aspect ratio *a/b* = 0.5; 1; 2; 4 and 7; a thickness-to-length ratio *a/h* = 10 and a volume fraction exponent *n* = 0.5 are taken. Apparently, varying the aspect ratio *a/b* leads to a strong increase in the dimensionless frequencies of FG plates. Furthermore, the first five modes of FG plates for *a/b* = 1 (square plate) and 4 (rectangular plate) are also depicted in Fig. 24, which shows a clear finite size effect on the mode-shapes of FG plate vibration.

Table 10

Effect of aspect ratio *a/b* on dimensionless frequencies of simply supported FG plates (*a/h* = 10, *n* = 0.5) made of ZrO_2/SUS304 obtained by the present method.

a/b	Mode 1	2	3	4	5
0.5	3.4967	5.5523	11.5024	13.3551	16.4725
1	5.5185	13.3327	20.4604	25.4576	31.6871
2	13.2002	20.3552	39.3487	44.8255	48.1604
4	38.9445	44.4674	65.4237	80.2463	96.3754
7	89.4794	93.0620	107.2442	117.7849	133.7789

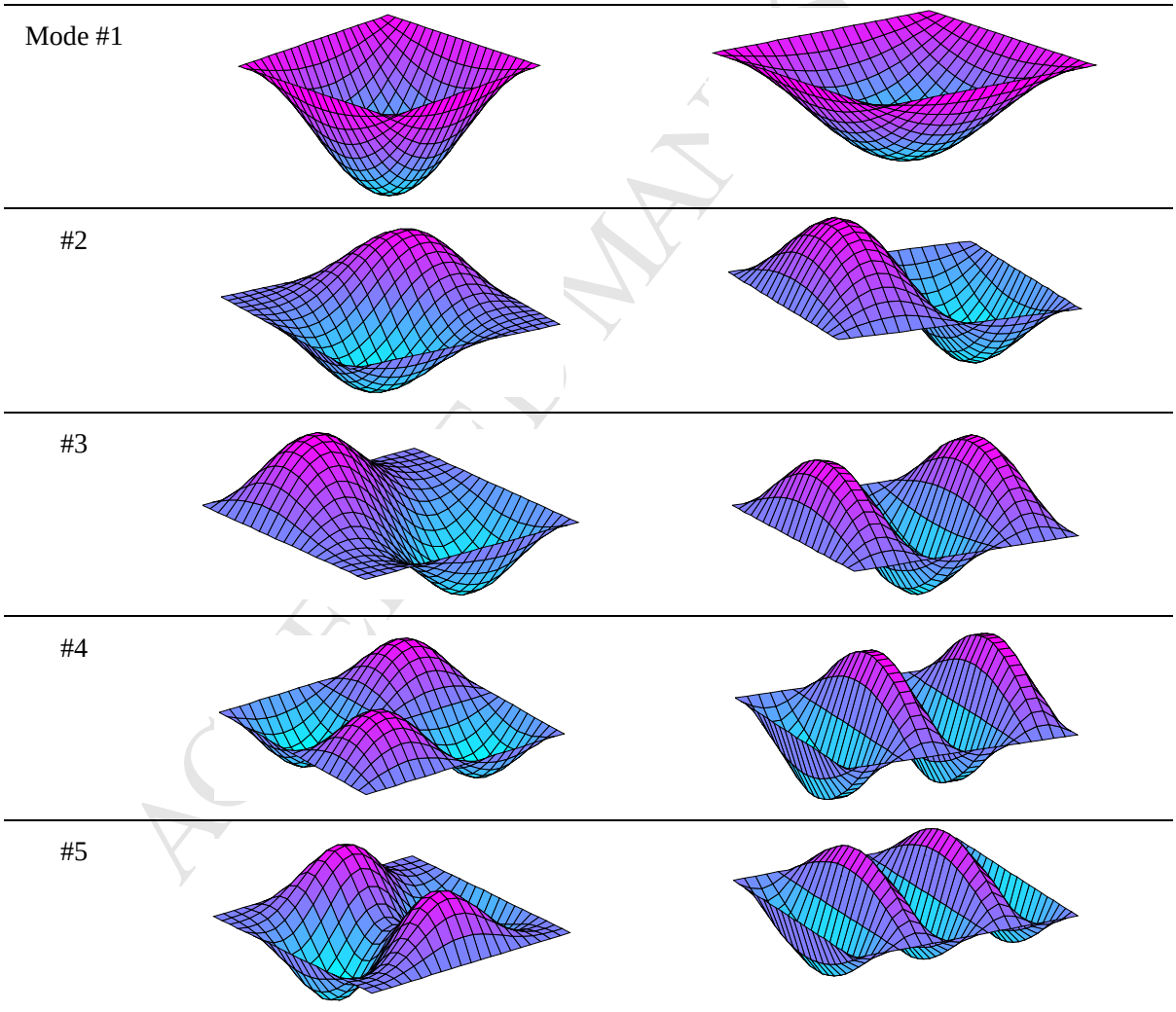

Fig. 24 Visualization of the first five mode-shapes of square (*a/b* = 1) and rectangular (*a/b* = 4) FG plates made of ZrO2/SUS304 (*a/h* = 10, *n* = 0.5) obtained by the developed EF model. .

4.2.2 A circle FG plate

Numerical results of the dimensionless natural frequencies for a simply supported circle FG plate (R/h = 10) made of Al_2O_3/SUS304 utilizing the present formulation are shown in Fig. 25. The normalized results of natural frequencies, $\Omega = \left(\omega\pi R^2/h\right)\left[\rho_0(1-\nu^2)/E_0\right]^{1/2}$, depicted in the figure are derived from two specified values of temperature, e.g., $T = 300K$ and $T = 1400K$. It is apparent that different environments of temperature lead to a significant variation of the natural frequencies of FG plates. The higher temperature the environments in which the plates locate the larger the natural frequencies are gained. In addition, the volume fraction exponent greatly alters the dimensionless frequencies as usual. Regardless of high temperature conditions, it is evident that the ceramic-rich plate always yield larger natural frequencies compared to plates whose properties are more and more metallic. Additionally, the first six modes of a simply supported circle FG plate with n = 0.5 under $T = 1400K$ are shown in Fig. 26.

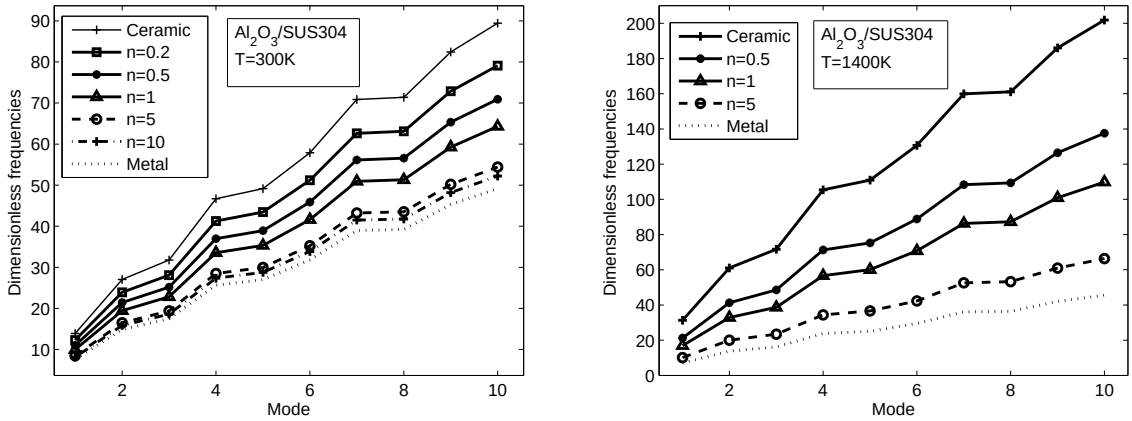

Fig. 25 Effect of volume fraction exponent on dimensionless frequencies of simply supported circled FG plates made of Al_2O_3/SUS304 for $T = 300K$ and $T = 1400K$ obtained by the developed model.

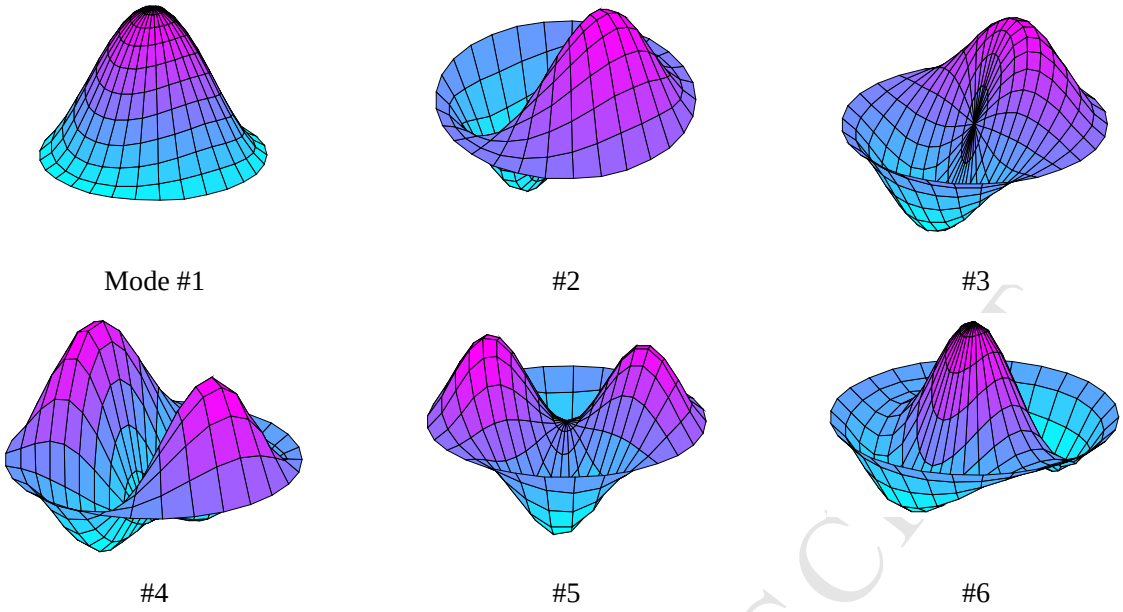

Fig. 26 Visualization of the first six modes of a simply supported circle FG plate (*R/h* = 10) made of Al_2O_3/SUS304 (*n* = 0.5) under $T = 1400K$ obtained by the developed model.

4.2.3 A L-shape FG plate

The last example for free vibration analysis is a simply supported L-shape FG plate (thickness *h* = 0.025m) made of ZrO_2/SUS304 under $T = 800K$. The first five modes of the natural frequencies of L-shape plate derived from the developed finite element model normalized by $\Omega = \left(3\omega L^2 / 4h\right)\left[\rho_0(1-\nu^2)/E_0\right]^{1/2}$ are then presented in Table 11, for different values of aspect ratio *L/b* and volume fraction coefficient *n*. In this example, we focus our interest only on the variation of the dimensionless frequencies affected by the aspect ratio *L/b* and the gradient index of FGMs. As a result, it is obvious that increasing the values of *L/b* leads to an increase of the frequencies. Once again, it can be observed in the table that the volume fraction exponent alters the dimensionless frequencies significantly as the ceramic-rich plates yield higher natural frequencies compared to pure metal plates and any other FG plates whose properties are more and more metallic. In other words, increasing the gradient index of FGMs leads to a decrease of the dimensionless frequencies of FG plates. The first five modes of simply supported L-shape

FG plates for different aspect ratios *L/b* =1; 2 and 3 are additionally depicted in Fig. 27. We again find out a significant effect of the aspect ratio *L/b* on the mode-shapes of FG plates.

Table 11

Dimensionless frequencies of simply supported L-shape FG plates (*h* = 0.025m) made of ZrO_2/SUS304 under $T = 800K$ obtained by the present method.

L/b	Mode	Ceramic	*n* = 0.5	*n* = 1	*n* = 5	Metal
1	1	14.5722	13.0582	12.4611	11.5820	11.4813
	2	17.1024	15.3270	14.6252	13.5898	13.4748
	3	21.7339	19.4819	18.5864	17.2604	17.1239
	4	33.0021	29.5771	28.2215	26.2208	26.0021
	5	39.0878	35.0337	33.4264	31.0513	30.7970
2	1	23.9924	21.5044	20.5179	19.0594	18.9035
	2	51.1614	45.8412	43.7486	40.6734	40.3099
	3	54.4484	48.7954	46.5605	43.2651	42.8996
	4	59.5040	53.3242	50.8846	47.2893	46.8829
	5	74.4241	66.7040	63.6453	59.1265	58.6383
3	1	37.1634	33.3084	31.7809	29.5243	29.2808
	2	74.4593	66.7354	63.6759	59.1560	58.6661
	3	107.0507	95.9121	91.5380	85.1182	84.3448
	4	109.0287	97.6921	93.2301	86.6722	85.9032
	5	131.7650	118.0798	112.6786	104.7195	103.8170

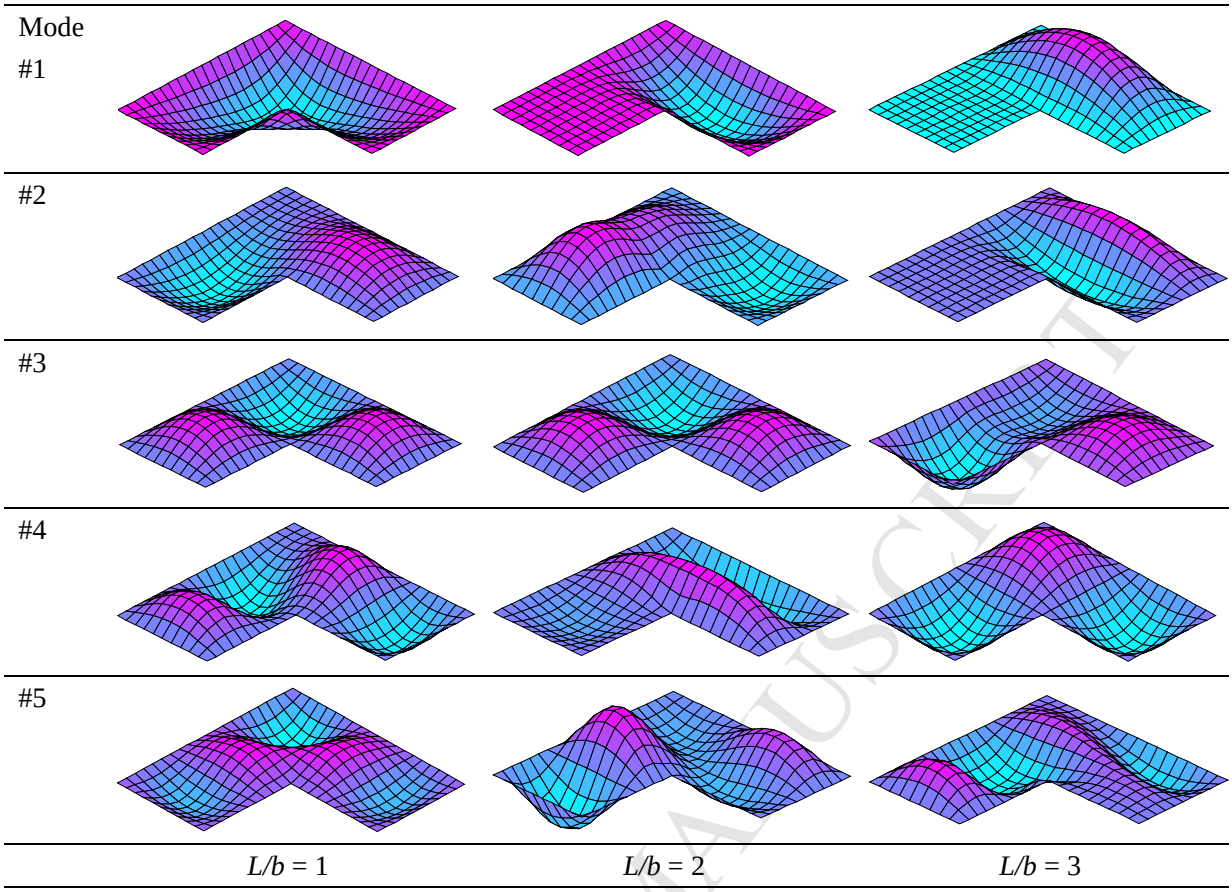

Fig. 27 Visualization of the first five modes of simply supported L-shape FG plate (h = 0.025m) made of ZrO_2/SUS304 (n = 0.5) under $T = 800K$ obtained by the developed model.

5. Conclusions and future works

In this paper, we present new numerical results for static bending and natural frequencies of FG plates with different configurations using a finite element formulation, taking the advantages of a new simple third order shear deformation plate theory (TSDT). The finite element formulation can be applied to deal with both thin and moderate thick FG plates without the need for special treatments of shear-locking effect and shear correction factors. The new TSDT that dominates over other existing theories is due to the fact that the theory is based on rigorous kinematic of displacements, deriving from an elasticity formulation rather than the hypothesis of displacements. The numerical results of static bending and natural frequencies obtained by this new TSDT theory are also compared to the solutions from other high order plate theories,

showing a good agreement among approaches. Some major conclusions drawn from the study can be summarized as follows:

- The subject under consideration on characterizing the high temperature mechanical behaviors of heated FG plates is important. The FGMs with excellent characteristics of ceramic in heat and corrosive resistances combined with the great toughness of metals in absorb energy and plastically deform, leading to outstanding advanced materials that can withstand large mechanical loads under high temperature environment. On the other hand, the plate structures in particular are one of major parts in many engineering applications. The use of plates or plate-like structures suffering high temperature conditions in nuclear power plant, aeronautical, civil, infrastructure, mechanical marine, and so on is very common in our modern life.
- Unlike the significant limitation of analytical approaches, the developed finite element model associated with a new simple TSDT makes it greatly effective in solving practical problems where complicated configurations are often encountered. The numerical results presented above have shown a high accuracy of the proposed numerical model, which can be considered as an effective numerical tool for extracting mechanical response of FG plates in high temperature environment.
- The mechanical behaviors of FG plates under consideration are complicated as they depend not only on the nonlinear thermal properties and behaviors of constituent materials but also on the volume fraction and material combinations. Static bending analysis has shown that the overall mechanical bending behaviors of FG plates are material-dependent, and more importantly, as it has been found that not all FG plates in high temperature environment

possess the same situation, they behave differently from each other, dependent on the constituent materials that form the FG plates. Obviously, the material combination is a crucial factor altering the overall mechanical behaviors of heated FG plates in high temperature. Particularly, numerical results accounted for FG plates made of Al_2O_3/SUS304, Si_3N_4/SUS304 and ZrO_2/SUS304 suffering high temperature condition indicate that, for instance, increasing the volume fraction exponent leads to an increase in mechanical deflections of the Al_2O_3/SUS304 and Si_3N_4/SUS304 plates, however it does not take place for the ZrO_2/SUS304 one. The ZrO_2/SUS304 plate inherently owns a more complicated mechanical behavior as it naturally generates a transition point in the response. This phenomenon may be useful to the designers and developers in a way of selection of appropriate constituent materials to form the FGMs, especially to which under tough conditions of high temperature. On the other hand, numerical results for eigenvalue analysis have shown that all FG plates yield a similar behavior. Generally, there are no significant differences on the natural frequencies for Al_2O_3/SUS304, Si_3N_4/SUS304 and ZrO_2/SUS304 plates. Loosely speaking, the natural frequencies of FG plates possess similar behaviors, regardless of the constituent materials being used to form the FG plates.

- Several aspect ratios including volume fraction coefficient, thickness-to-length, size effect, temperature, boundary conditions, material combinations, etc., which have significant impacts on the mechanical behaviors of deflections and natural frequencies of FG plates.
- The present formulation is general and has no limitations to extend it to other problems related to plates or plate-like structures especially those in high temperature environment. Among others the nonlinear vibration of FG plates and shells, sandwich FG plates, buckling

of imperfect FG plates, etc. in high temperature would be very interesting. For instance, we may apply the proposed method to model thermal buckling of annular microstructure-dependent FGM plates resting on an elastic medium [30]; functionally graded carbon nanotube-reinforced cylindrical panel subjected to thermo-mechanical load [31]; and thermal buckling of grid-stiffened FGM cylindrical shells [32]. Other numerical approaches for modeling cracked FG plates in high temperature, for instance, the meshfree methods [33-35], the extended plate finite element [2, 36], or the extended isogeometric analysis [37-38] would be potential.

Acknowledgment

TQB and SH gratefully acknowledge the support of the Grant-in-Aid for Scientific Research (No. 26-04055) - JSPS (No. P14055). DHD also gratefully acknowledges the support of the Grant-in-Aid for Scientific Research (No. 26-04049) - JSPS (No. P.14049).

References

[1]. Khor AK, Dong LZ, Gu WY. Plasma sprayed functionally graded thermal barrier coatings. Mater. Lett. 38 (1999) 437-444.

[2]. Liu P, Bui TQ, Zhu D, Yu TT, Wang JW, Yin SH, Hirose S. Buckling failure analysis of cracked functionally graded plates by a stabilized discrete shear gap extended 3-node triangular plate element. Composites Part B. 77 (2015) 179-193.

[3]. Wattanasakulpong N, Prusty GB, Kelly DW. Free and forced vibration analysis using improved third-order shear deformation theory for functionally graded plates under high temperature loading. J. Sandw. Struct. Mater. 15 (2013) 583-606.

[4]. Huang XL, Shen HS. Nonlinear vibration and dynamic response of functionally graded plates in thermal environments. Int. J. Solids Struct. 41 (2004) 2403-2427.

[5]. Wattanasakulpong N, Prusty GB, Kelly DW. Thermal buckling and elastic vibration of third-order shear deformable functionally graded beams. Int. J. Mech. Sci. 53 (2011) 734-743.

[6]. Shi G. A new simple third-order shear deformation theory of plates. Int. J. Solids Struct. 44 (2007) 4399-4417.

[7]. Yang J, Shen HS. Nonlinear bending analysis of shear deformable functionally graded plates subjected to thermo-mechanical loads under various boundary conditions. Composites Part B: Eng. 34 (2003) 103-115.

[8]. Shen SH. Nonlinear bending response of functionally graded plates subjected to transverse loads and in thermal environments. Int. J. Mech. Sci. 44 (2002) 561-584.

[9]. Yang J, Shen SH. Vibration characteristic and transient response of shear deformable functionally graded plates in thermal environments. J. Sound Vib. 255 (2002) 579-602

[10]. Talha M, Singh BN. Static response and free vibration analysis of FGM plates using higher order shear deformation theory. Appl. Math. Modell. 34 (2010) 3991-4011.

[11]. Tanigawa Y, Akai T, Kawamura R, Oka N. Transient heat conduction and thermal stress problems of nonhomogeneous plate with temperature-dependent material properties. J. Ther. Stre. 19 (1996) 77-102.

[12]. Samsam Shariat BA, Eslami MR. Thermal buckling of imperfect functionally graded plates. Int. J. Solids Struct. 43 (2006) 4082-4096.

[13]. Aboudi J, Arbold SM, Pindera MJ. Response of functionally graded composites to thermal gradients. Composites Eng. 4 (1994) 1-18.

[14]. Kim KS, Noda N. A Green's function approach to the deflection of a FGM plate under transient thermal loading. Arch. Appl. Mech. 72 (2002) 127-137.

[15]. Golmakani ME, Kadkhodayan M. Large deformation analysis of circular and annular FGM plates under thermo-mechanical loadings with temperature-dependent properties. Composites Part B: 42 (2011) 614-625.

[16]. Jha DK, Kant T, Singh RK. A critical review of recent research on functionally graded plates. Composit. Struct. 96 (2013) 833-849.

[17]. Thai HT, Kim SE. A review of theories for the modeling and analysis of functionally graded plates and shells. Composit. Struct. 128 (2015) 70-86.

[18]. Yu TT, Yin SH, Bui QT, Hirose S. A simple FSDT-based isogeometric analysis for geometrically nonlinear analysis of functionally graded plates. Finit. Elemt. Anal. Des. 96 (2015) 1-10.

[19]. Yin SH, Hale JS, Yu TT, Bui QT, Bordas SPA. Isogeometric locking-free plate element: a simple

first order shear deformation theory for functionally graded plates. Composit. Struct. 118 (2015) 121-138.

[20]. Yin SH, Yu YY, Bui QT, Nguyen NM. Geometrically nonlinear analysis of functionally graded plates using isogeometric analysis. Eng. Comput. 32 (2015) 519-558.

[21]. Valizadeh N, Natarajan S, Gonzalez-Estrada OA, Rabczuk T, Bui QT, Bordas PAS. NURBS-based finite element analysis of functionally graded plates: Static bending, vibration, buckling and flutter. Composit. Struct. 99 (2013) 309-326.

[22]. Bhardwaj G, Singh IV, Mishra BK, Bui QT. Numerical simulation of functionally graded cracked plates using NURBS based XIGA under different loads and boundary conditions. Composit. Struct. 126 (2015) 347-359.

[23]. Thai HT, Vo PT, Bui QT, Nguyen TK. A quasi-3D hyperbolic shear deformation theory for functionally graded plates. Acta Mech. 225 (2014) 951-964.

[24]. Bui QT, Khosravifard A, Zhang Ch, Hematiyan MR, Golub MV. Dynamic analysis of sandwich beams with functionally graded core using a truly meshfree radial point interpolation method. Eng. Struct. 47 (2013) 90-104.

[25]. Malekzadeh P, Shojaee SA. Dynamic response of functionally graded plates under moving heat source. Composites Part B. 44 (2013) 295-303.

[26]. Malekzadeh P, Monajjemzadeh SM. Dynamic response of functionally graded plates in thermal environmental under moving load. Composites Part B. 45 (2013) 1521-1533.

[27]. Reddy JN. Analysis of functionally graded plates. Int. J. Numer. Meth. Eng. 47 (2000) 663-684.

[28]. Zenkour AM. Generalized shear deformation theory for bending analysis of functionally graded plates. Appl. Math. Model. 30 (2006) 67-84.

[29]. Daouadji TH, Tounsi A, Bedia EAA. Analytical solution for bending analysis of functionally graded plates. Scientia Iranica B 20 (2013) 516-523.

[30]. Ashoori AR, Vanini SAS. Thermal buckling of annular microstructure-dependent functionally graded material plates resting on an elastic medium. Composites Part B. 87 (2016) 245-255.

[31]. Alibeigloo A. Elasticity solution of functionally graded carbon nanotube-reinforced composite cylindrical panel subjected to thermomechanical load. Composites Part B. 87 (2016) 214-226.

[32]. Sun J, Lim CW, Xu SH, Mao H. Accurate buckling solutions of grid-stiffened functionally graded cylindrical shells under compressive and thermal loads. Composites Part B. 89 (2016)

96-107.

[33]. Tanaka S, Suzuki H, Sadamoto S, Imachi M. Bui QT. Analysis of cracked shear deformable plates by an effective meshfree plate formulation. Eng. Fract. Mech. 144 (2015) 142-157.

[34]. Bui QT, Nguyen NM, Zhang Ch. A meshfree model without shear-locking for free vibration analysis of first-order shear deformable plates. Eng. Struct. 33 (2011) 3364-3380.

[35]. Bui QT, Nguyen NM. A moving Kriging interpolation-based meshfree method for free vibration analysis of Kirchhoff plate. Comput. Struct. 89 (2011) 380-394.

[36]. Yu TT, Bui QT, Liu P, Hirose S. A stabilized discrete shear gap extended finite element for the analysis of cracked Reissner-Mindlin plate vibration problems involving distorted meshes. Int. J. Mech. Des. (2015) in press, http://dx.doi.org/10.1007/s10999-014-9282-x.

[37]. Bui QT. Extended isogeometric dynamic and static fracture analysis for cracks in piezoelectric materials using NURBS. Comput. Meth. Appl. Mech. Eng. 295 (2015) 470-509.

[38]. Yu TT, Bui QT, Yin SH, Doan HD, Wu CT, Do VT, Tanaka S. On the thermal buckling analysis of functionally graded plates with internal defects using extended isogeometric analysis. Compo. Struct. 136 (2016) 684-695.